Article

Months-long thousand-kilometre-scale wobbling before great subduction earthquakes

https://doi.org/10.1038/s41586-020-2212-1

Received: 17 May 2019

Accepted: 5 February 2020

Published online: 29 April 2020

Check for updates

Jonathan R. Bedford[1]✉, Marcos Moreno[2], Zhiguo Deng[1], Onno Oncken[1,3], Bernd Schurr[1], Timm John[3], Juan Carlos Báez[4] & Michael Bevis[5]

Megathrust earthquakes are responsible for some of the most devastating natural disasters[1]. To better understand the physical mechanisms of earthquake generation, subduction zones worldwide are continuously monitored with geophysical instrumentation. One key strategy is to install stations that record signals from Global Navigation Satellite Systems[2,3] (GNSS), enabling us to track the non-steady surface motion of the subducting and overriding plates before, during and after the largest events[4–6]. Here we use a recently developed trajectory modelling approach[7] that is designed to isolate secular tectonic motions from the daily GNSS time series to show that the 2010 Maule, Chile (moment magnitude 8.8) and 2011 Tohoku-oki, Japan (moment magnitude 9.0) earthquakes were preceded by reversals of 4–8 millimetres in surface displacement that lasted several months and spanned thousands of kilometres. Modelling of the surface displacement reversal that occurred before the Tohoku-oki earthquake suggests an initial slow slip followed by a sudden pulldown of the Philippine Sea slab so rapid that it caused a viscoelastic rebound across the whole of Japan. Therefore, to understand better when large earthquakes are imminent, we must consider not only the evolution of plate interface frictional processes but also the dynamic boundary conditions from deeper subduction processes, such as sudden densification of metastable slab.

Much of the research into earthquake hazard focuses on approximating the magnitudes of the next large earthquakes and estimating when they may occur. Accordingly, regions of the subduction interface that are estimated to have accumulated enough elastic potential energy to match previous earthquakes in that location are considered to be mature segments where a major earthquake can be considered overdue[8]. This hazard assessment is limited by our ability to estimate the long-term relative velocities of the subducting and overriding plates, especially if most of the accumulation period has occurred over times when no modern geophysical instrumentation was deployed. Recently, it has been discovered that relative plate velocities recorded by GNSS vary not only as a postseismic reaction to large earthquakes at neighbouring segments of the subduction plate interface[4–6], but also at mature segments years to days before the onset of main earthquake ruptures[9–11]. Such precursory motions, recorded on the overriding plate surface, are thought to be related to a gradual evolution of stress conditions on the plate interface leading to mainshock failure, which sometimes occurs as a cascading series of foreshocks and respective foreshock afterslips[9] and other times as accelerating aseismic creep[12]. Earthquake precursory phenomena have been extensively studied in laboratory shearing experiments and consist of noticeable changes in acoustic emissions and fluctuation in the measured stress[13,14].

To ascertain the prevalence of tectonic transients in fault zones, we need methods that distinguish the purely tectonic motion from the other non-tectonic signals and artefacts in the continuous GNSS time series[15]. A recently developed time series regression approach called Greedy Automatic Signal Decomposition (GrAtSiD)[7] allows for the automatic estimation of variable interseismic motions at GNSS stations. This technique models the interseismic motions as the sum of a slope, an offset and a sparse number of transient functions (for example, exponential decays; see Methods).

We applied GrAtSiD to continuous GNSS time series in the broad regions of the M_w 8.8 Maule, Chile, 2010 and M_w 9.0 Tohoku-oki, Japan, 2011 earthquakes (hereafter referred to as the Maule and Tohoku-oki earthquakes, respectively) (Fig. 1 and Extended Data Fig. 1), outputting a modelled trajectory for each directional component of the time series that has been separated from jumps (both tectonic and non-tectonic) and steady-state seasonal oscillations (Methods). To interpret this variable interseismic trend it is crucial to identify the sources of non-tectonic signals that may be present in the original time series. By comparing the transient signals of interest (that have been

[1]Helmholtz Centre Potsdam, GFZ German Research Centre for Geosciences, Potsdam, Germany. [2]Departamento de Geofísica, Universidad de Concepción, Concepción, Chile. [3]Institute of Geological Sciences, Freie Universität Berlin, Berlin, Germany. [4]University of Chile, National Seismological Centre, Santiago, Chile. [5]School of Earth Sciences, Ohio State University, Columbus, OH, USA. ✉e-mail: jbed@gfz-potsdam.de

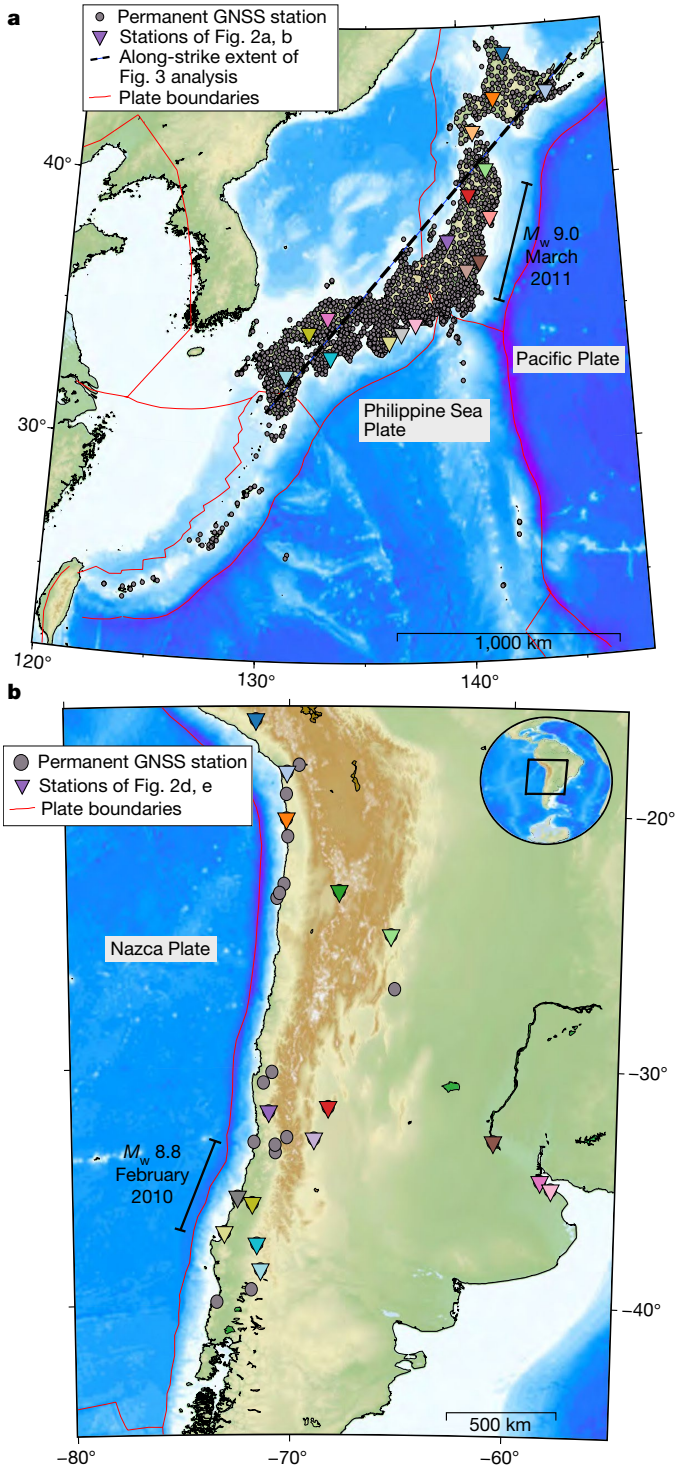

Fig. 1 | Locations of the great earthquakes and of the continuous GNSS stations that capture the preceding transient motions. a, Continuous GNSS stations (grey dots) used in this study. Inverted triangles indicate stations whose time series are shown in Fig. 2 (corresponding to coloured time series). The dashed black line is used in the along-strike analysis of Fig. 3. **b**, As for **a**, but for the South American stations in the region of the Maule earthquake.

isolated by GrAtSiD) to time series predicted from the fluid loading (atmospheric, hydrological and oceanic)[16], and also by analysing the lateral extent of the transient signals (to probe a possible reference frame explanation), we determine that the source of these signals is most likely to be of tectonic origin (Methods).

Features of the modelled trajectories

Figure 2 shows the detrended displacement time series before and after the removal of background seasonal oscillation[17,18] and common-mode errors[19]. We can clearly see that there are variable interseismic rates and strong accelerations in the months leading up to both great earthquakes. The application of GrAtSiD has reduced the noise (seasonal and common-mode) that otherwise obscures this non-steady signal (see also Methods, Extended Data Figs. 2 and 3, and Supplementary Videos 1 and 2). Various transient motions exist in the time series, but the most prominent and long-lived episodes are those in the final 5 and 7 months before the Tohoku-oki and Maule earthquakes, respectively, during which the peak-to-peak amplitude of the horizontal reversals range between 4 mm and 8 mm. These anomalous reversal signals before the Tohoku-oki earthquake are prominent even in the non-filtered time series, whereas before the Maule earthquake, one can clearly see the reversals only after the removal of the seasonal. Before the Tohoku-oki earthquake, there is an earlier, milder reversing signal beginning approximately 19–20 months before the mainshock that shares many spatial characteristics with the later, faster reversals (Supplementary Video 3). Owing to their appearance in the time series, we also refer to these fast reversals in surface motion as 'wobbles'. Before both earthquakes, the approximate azimuth of the horizontal reversal is perpendicular to the strike of the earthquake focal mechanism, which strongly suggests a tectonic origin for the transient signal.

Given the exceptionally dense station spacing in Japan, we were able to perform an along-strike analysis of the transient velocity field along the whole subduction zone (Fig. 3). Although there is some variation of the interseismic velocity along the subduction margin, there is a strong wobbling beginning in October 2010 and lasting until the onset of the Tohoku-oki earthquake in March 2011. A zoom-in on this time window shows that, in the East component, there is a migration of the velocity front across the Earth's surface of approximately 1,000 km in a fortnight (a rate of about 3 km h^{-1}). This velocity front propagates along Japan from the southwest and seems to start as far away as near Taiwan (Supplementary Videos 3 and 4). Because there are fewer stations in the South American network, it is harder to track a velocity front before Maule, although we are able to see a mostly East–West wobbling along Chile in the months preceding the Maule earthquake (Fig. 4, Supplementary Videos 5 and 6). We note also that the Maule reversal in Fig. 4 looks noisier than the Japanese reversal in Fig. 3c. This is because the pre-Maule case has far fewer stations and so we are not able to spatially average the detrended displacements. Before the Tohoku-oki earthquake, anomalous wobbling occurs in both the vertical and horizontal components (Fig. 3, Extended Data Figs. 2 and 4), whereas before the Maule earthquake, the wobbling is mainly in the East–West direction. In the Argentinian stations, there is a strong transient subsidence beginning 4–5 months before the Maule earthquake that persists until the rupture (Figs. 2, 4, Extended Data Fig. 3 and Supplementary Video 6).

Comparison with previous studies

We hereafter refer to the wobbling periods 5 and 7 months before the Tohoku-oki and Maule earthquakes, respectively, as the unstable periods. In previous studies of both mainshocks, precursory seismic periods have been reported: before the Maule earthquake, anomalous shallow (≤40 km) and deep (≥80 km) seismicity occurred within 0.5° of the mainshock hypocentre, beginning approximately 40 days before the mainshock[20]. Before the Tohoku-oki earthquake, a foreshock phase is reported to have begun in late November 2010[21] within 2° of the mainshock epicentre and with an enhanced rate of deeper (≥80 km) seismic moment release at approximately 60 days before the mainshock[20]. Slow slip, inferred from repeating earthquake analysis[21], an onshore volumetric strainmeter[22] and ocean-bottom pressure time series[22], is thought to have begun around 1 month before the Tohoku-oki earthquake and

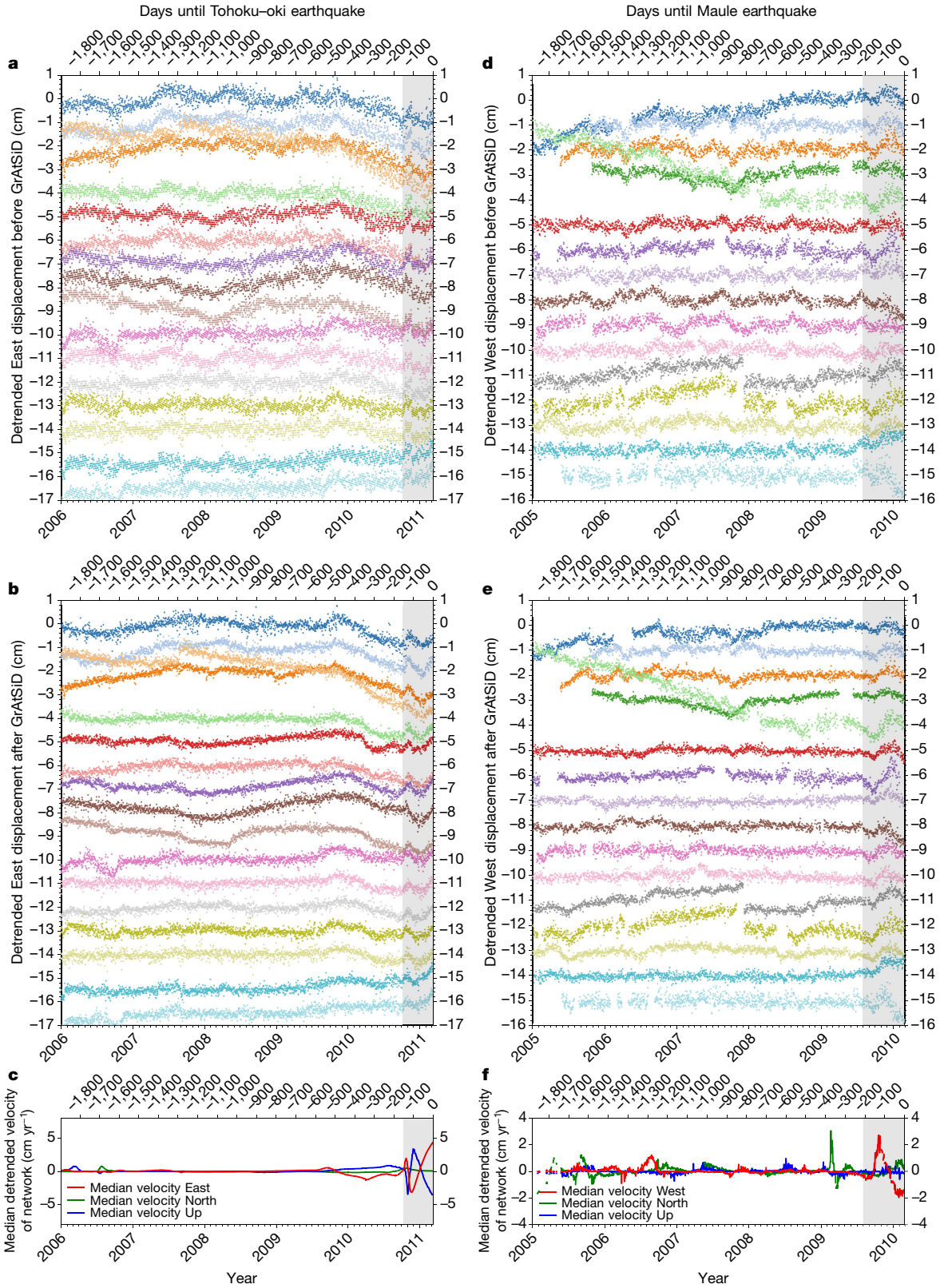

Fig. 2 | Time series before Tohoku-oki and Maule and the effect of noise removal with GrAtSiD. a, East displacement time series before the 2011 Tohoku-oki earthquake (colours going from top to bottom correspond to locations of coloured triangles on Fig. 1 going from north to south). Time series have been manually detrended for optimal display. Offsets (steps) in these time series (automatically solved by GrAtSiD) have been removed. **b**, Time series from panel **a** after removal of background, fluid-loading-induced seasonal oscillations (annual and semi-annual) and network-correlated daily noise (common-mode error). See Extended Data Figs. 2 and 3 for time series before GrAtSiD processing. The grey shading on the right indicates the unstable period before the mainshock. **c**, Average (median) deviation from median velocity at each station of the Japanese network, where median velocity of each station is determined between 1 January 2006 and 8 March 2011. **d**, **e**, As for **a** and **b**, except for the South American stations shown on Fig. 1 and in the West (mainly trenchward) direction. **f**, As for **c**, but for the South American data. Median station velocities calculated between 1 January 2005 and 25 February 2010. We note that in both **c** and **f**, the average deviation from background velocity is only calculated if more than 55% of stations have data on that particular day.

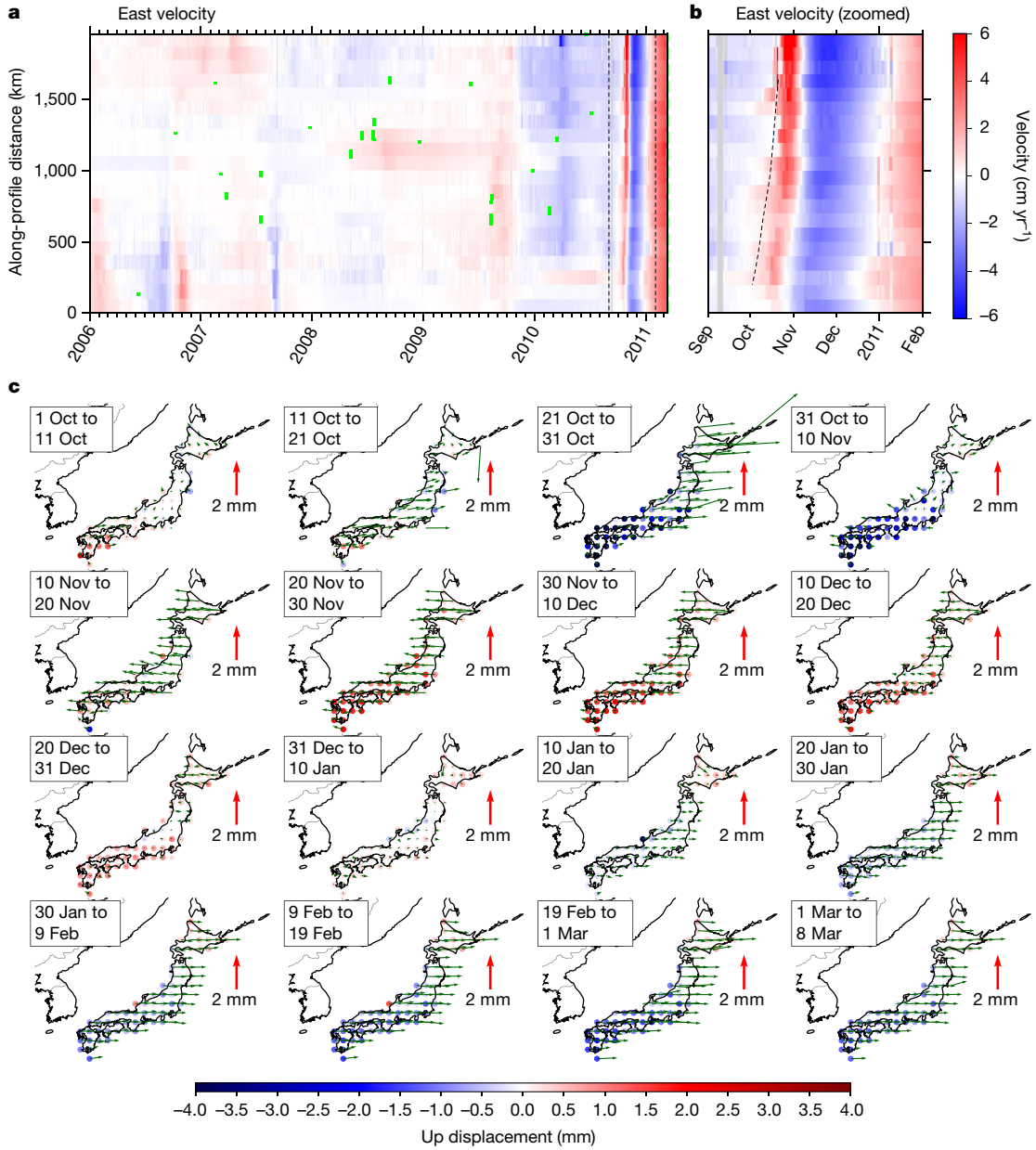

Fig. 3 | Visualizing the along-strike signal migration and reversal of Japan in the years and months preceding the Tohoku-oki earthquake. a, Table of velocities (East component) within non-overlapping rectangular regions before the Tohoku-oki earthquake. Velocity for each station within each rectangular region is detrended relative to the median velocity of that station between 1 January 2006 and 8 March 2011. The medians of these detrended velocities are then chosen as the representative regional velocities. The *y* axis indicates distance in the northeast direction for the centroid of each rectangular region of Fig. 1 (beginning in the southwest). Green lines indicate the along-strike locations and times of earthquakes exceeding moment magnitude 6. **b**, A zoom-in of panel **a**, between the beginning of September 2010 and the beginning of February 2011 (dashed vertical black lines on panel **a**). The dashed line on panel **b** indicates the velocity front that migrates across Japan from the southwest. **c**, Snapshots of median displacement for stations within 1° squares (after detrending each time series) for 10-day windows from October 2010 until the Tohoku-oki earthquake (see also Supplementary Video 4, which covers this period). Green arrows indicate horizontal displacements and coloured circles indicate vertical displacements. The period covered by snapshots is the unstable period described in this study.

within the extent of the mainshock source area, whereas seismic tremor is reported as having begun in late January 2011 within 100 km of the Tohoku-oki mainshock hypocentre[23,24]. The stress field in the crust above the Tohoku-oki mainshock slip area, as determined by analysis of focal mechanisms[25], shows a gradual reduction in compression over three years in the run-up to the mainshock, although the time resolution of this reduction is limited by the number of large enough earthquakes.

Previous studies in which pre-Tohoku-oki surface trajectories were modelled[10,11,26] suggest a gradual acceleration in uncoupling of the plate interface near the mainshock region over the decade preceding the mainshock, although these analyses have not extended far beyond the mainshock rupture extents. There are no previous reports of precursory continental surface motions preceding the Maule earthquake. Although able to capture the main decadal-scale features, previous efforts to characterize secular tectonic velocity changes leading up to the Tohoku-oki and Maule earthquakes have been hindered by the need for iterative, manual improvements of the trajectory model. With GrAtSiD, we have been able to identify the subtle transients in the time series across the whole Japanese and South American networks that would have taken an unreasonable amount of time without an automated approach.

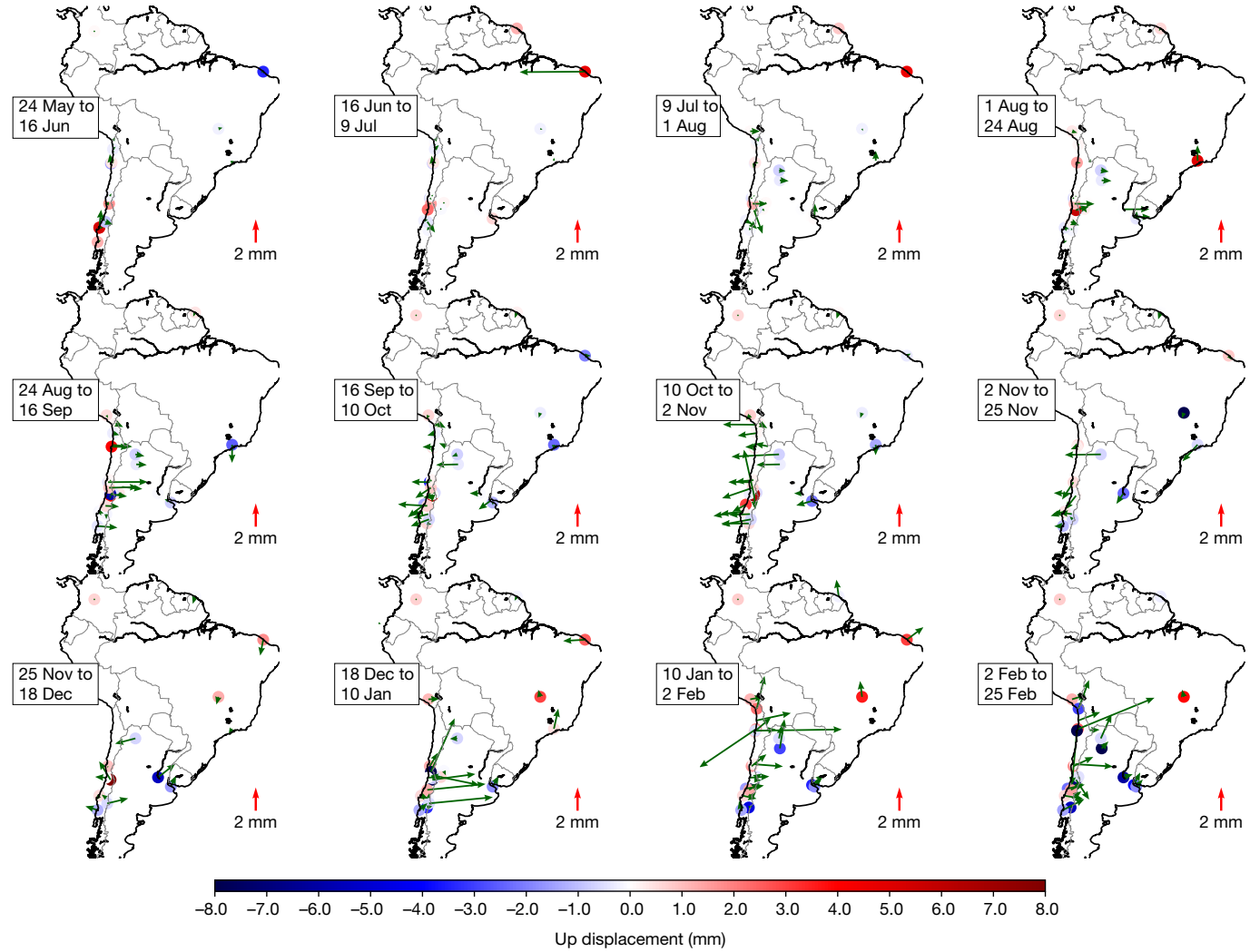

Fig. 4 | Visualizing the reversals motions in South America in the months preceding the Maule earthquake. Snapshots of displacement (after detrending) for 23-day windows from 279 days until 2 days before the Maule Earthquake. This time period covers the unstable period described in our study. Green arrows indicate horizontal displacement and coloured circles indicate vertical displacement.

Investigation of deformation mechanisms

To investigate the physical processes responsible for the pre-Tohoku-oki unstable period, we modelled the displacements (obtained from the trajectory modelling) using a simple elastic dislocation approach[27,28] (Methods). The model supports the possibility of an initial migration of slip across the subduction interface and indicates that the unstable period began with a large slab extension localized in the downgoing Philippine Sea Plate (Fig. 5 and Supplementary Video 7). This proposed slow slip across the margin is apparent from the general increase in apparent slip along the fault model from southwest to northeast. The occurrence of slow slip is also supported by similar propagation velocities (a few kilometres per hour) of the signal along the continental surface that have been observed in the Cascadia subduction zone[29] and the Nankai Trough[30]. Furthermore, the velocities of the in situ slip (of the order of 1 mm per day) match the velocities expected for slow-slip events[31]. The extension appears in the simplified dislocation model as an apparent simultaneous shallow updip slip and deep downdip locking (backslip[32]) centred at approximately 50–100 km. Following this extension, the surface velocity swings between pointing at the subduction trench, towards Eurasia, and then again towards the subduction trench. During this swing, the elastic dislocation model seems to indicate that the plate interface switches between enhanced locking and creeping: a more likely explanation is that the model is incorrectly projecting deformation of a viscoelastic rebound to the sudden extension. Figure 6 illustrates the possible series of events in the pre-Tohoku-oki unstable period. The initial slow-slip migration from the southwest to northeast of the study region is possibly facilitated by fluid release onto the plate interface. Seismic tomography of the downgoing Philippine Sea Plate[33] shows Poisson's ratio values that indicate a slab with fluid-filled porosity at the depths where we suspect slow slip to have begun and where extension is thought to be centred. Tomography of the Pacific slab also indicates sufficient fluids from the depth of the continental Mohorovičić discontinuity (Moho)[34] and shallower[35]. Such an expulsion of fluids and propagation of the slow slip would be supported by geological evidence for chemical mineral reactions. These reactions, that typically last between one and four months[36], produce pulse-like slab dehydrations that in turn suddenly increase pore-fluid pressure, thereby causing a feedback effect that mechanically weakens the plate interface[31,36,37]. This timescale, taken as an upper bound on the duration of these processes, fits the timescale of the suspected slow-slip duration that we describe in this study.

We hypothesize that the sudden extension that began towards the end of October could have been caused by either eclogitization of the slab just below the extension centre (for example, 50–100 km), or deeper slab pulling. Eclogitization processes can be rapid and mostly aseismic under thermodynamically overstepped conditions[36,38] in which pressure and

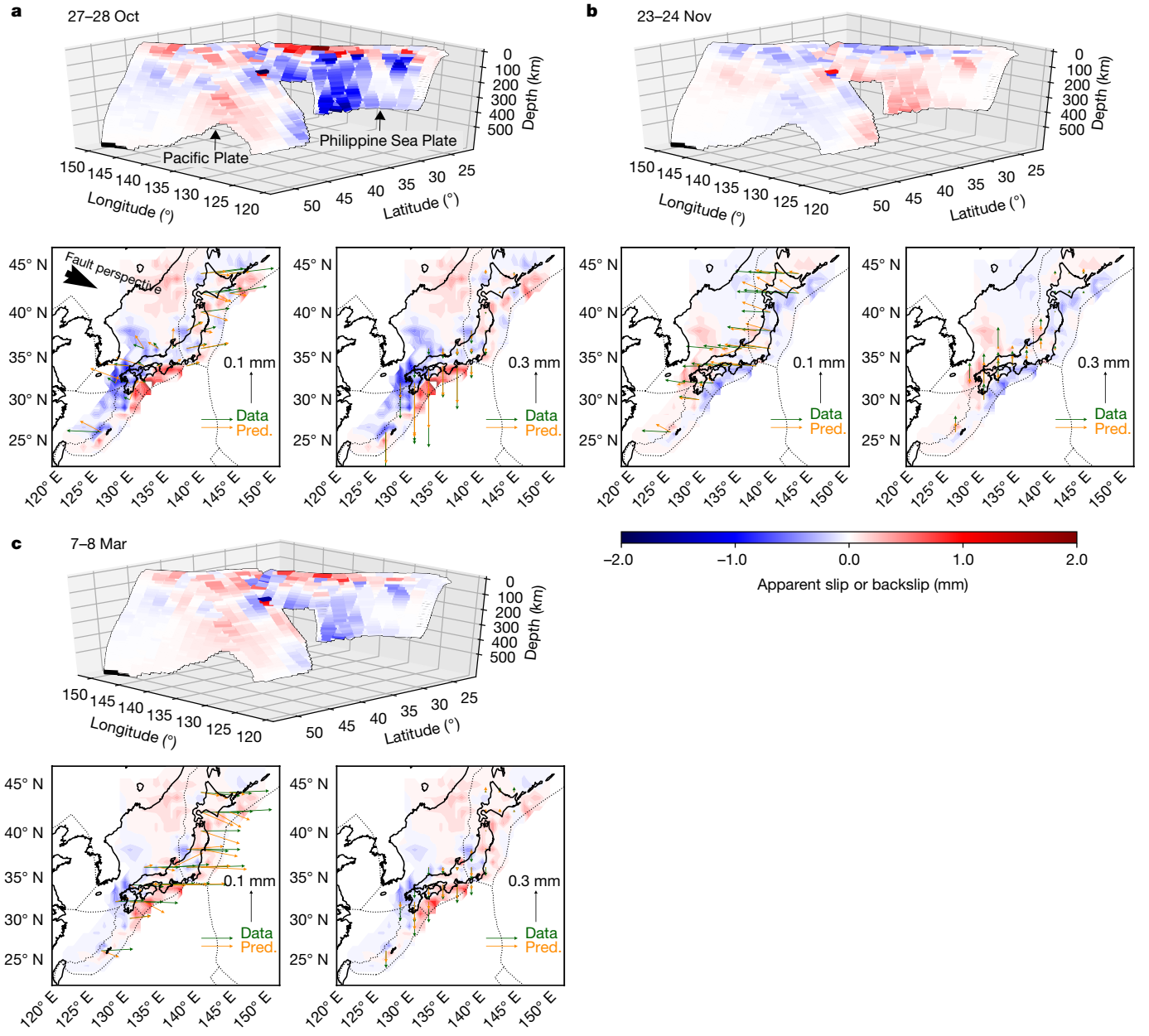

Fig. 5 | Surface velocities and kinematic models of apparent slip or backslip for three daily time windows during the unstable period preceding the Tohoku-oki earthquake. The date of the daily model is indicated above the view of the fault (all frames from September 2010 onwards are shown in Supplementary Video 8). Corresponding data and model predictions (for horizontal and vertical displacements) are shown in the maps underneath each view of the fault. The fault consists of two downgoing oceanic slabs in contact with the overriding continental plate: the Pacific Plate to the northeast and the Philippine Sea Plate to the southwest. On 27 October (**a**), the Philippine Sea Plate seems to be in a state of extension centred at approximately 50 km depth, as indicated by the updip positive and downdip negative dislocation pattern. Comparing the modelled kinematics of 23 November (**b**) and 7 March (**c**) (top right and bottom left subsets) we can see that the sense of dislocation is reversed for data displacements that are also approximately reversed. The junction between the two downgoing slabs also seems to demarcate a change in kinematics throughout all of the unstable phase. We note that the oscillating signal following the sudden pulldown (extension) is probably not well modelled by elastic dislocation. The apparent switch between enhanced locking, creeping and locking is likely to be an artefact of the elastic dislocation approach, which models the suspected viscoelastic response of the subduction zone as a purely plate interface process.

temperature make the reaction energetically favourable but sufficient activation energy for the initial reaction has been lacking. Conditions for fast eclogitization would require metastable regions in the downgoing slab, which receive infiltration of external fluid to overcome sluggish kinetics[39,40]. Although the presence of fluids—a catalyst for such a sudden densification to occur—is highly likely[33], the volume of metastable slab material (lower-crustal gabbroic rocks) in the Philippine Sea slab at depths of approximately 50–100 km is not known and, owing to the rather slow spreading of the related ridge (about 4 cm yr^{-1})[41], is expected to be small[42].

An alternative to pull from fast eclogitization is that the sudden pull comes from a deeper source. From the dislocation modelling, it is not clear if this initial downward slab pull has a shallow or deep origin. Figure 5 and Supplementary Video 7 show that the largest values of apparent enhanced locking are usually in the deepest patches of the model (approximately 400 km) on the Philippine Sea Plate interface. A possible

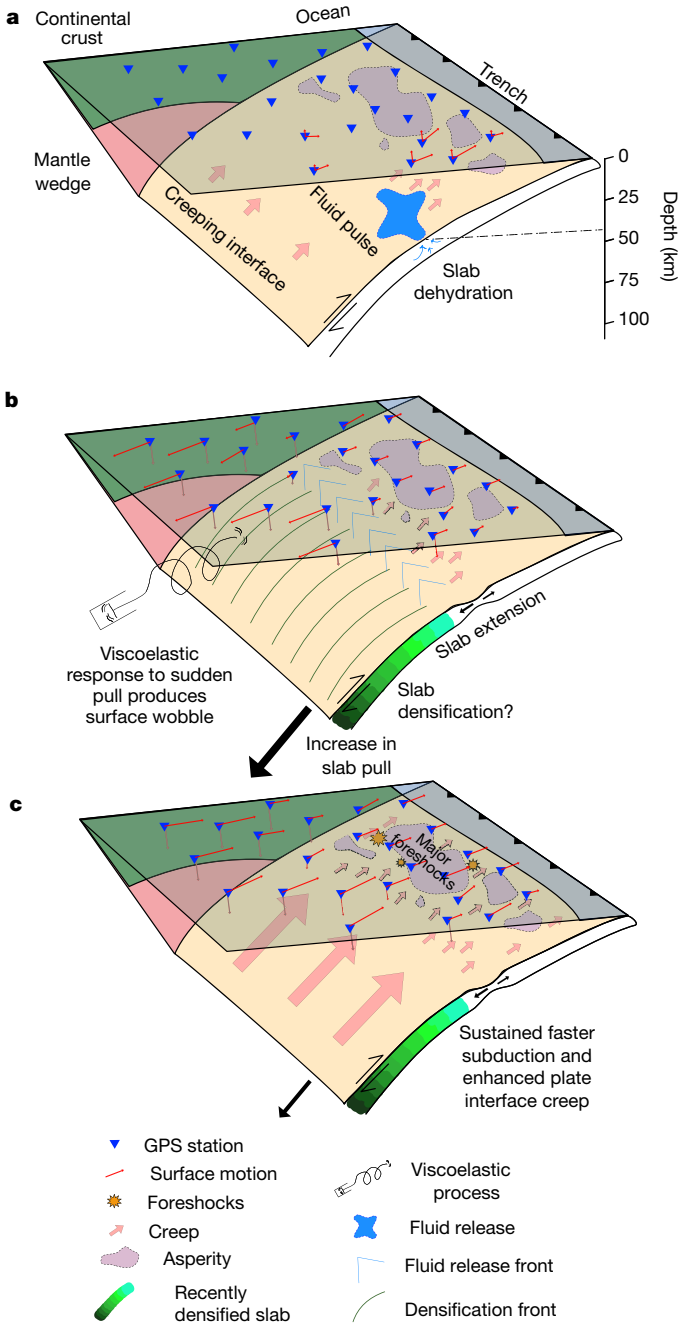

Fig. 6 | Cartoon (not to scale) to illustrate the possible processes explaining the deformation recorded in the unstable period captured before the Tohoku-oki earthquake. a, An initial pulse of fluids is released onto the plate interface via intraslab fluid pathways and dehydration reactions. This facilitates a slow-slip event caused by a reduction in the effective coefficient of friction. **b**, Slow-slip front migrates along strike. Sudden slab densification occurs and creates a buoyancy instability and enhanced downwards pull. This initial downwards acceleration causes slab extension and a quasidynamic wobbling of the subduction zone as the slab viscoelastically rebounds. Slab extension also results in faster creep downdip of the seismogenic zone and below the continental Moho. **c**, The slab extension continues, resulting in prolonged deep slip. The sudden slab pull and viscoelastic response, along with the large slow slip facilitated by fluid release has resulted in enhanced creep in the seismogenic zone that critically stresses a configuration of mature asperities, resulting in large foreshocks and the mainshock Tohoku-Oki M_w 9.0 earthquake.

mechanism to explain this deeper pull would be buoyancy instability caused by a sudden densification of slab material from alpha-olivine into beta-olivine or even gamma-olivine (that is, wadsleyite and ringwoodite formation) as it moves through the mantle transition zone at depths of 410 km and 660 km (ref. [43]). Intrinsic chemical heterogeneities would cause the reaction to start at spatially heterogeneously distributed locations within the slab; the reaction would then spread with increasing velocity owing to the exothermic reaction and resulting densification[43]. The sudden increase of slab pull would cause a perturbation of the force equilibrium at the plate interface sufficient to trigger a nonlinear response such as shear-heating-related slip acceleration or a power-law stress-dependent creep[44], which by its nature is a transient phenomenon.

From the tomography[45], the Philippine Sea Plate at mantle transition-zone depths seems to be in contact with (or in close proximity to) the slab of the metastable Pacific Plate[46], which has subducted under the Philippine Sea Plate in a flat fashion[45]. Therefore, it could be the sudden densification of metastable material in the Pacific slab and its subsequent dragging against the Philippine Sea slab that has caused the increased slab pull. Related to this possibility of slab communication, the dislocation model (Fig. 5 and Supplementary Video 7) suggests an interaction between downgoing slabs at their lateral juncture—whereby it seems that the plunging Philippine Sea Plate has dragged the Pacific Plate, which also appears to undergo some extension in the unstable period. This slab communication, however, is only apparent from the simple dislocation model, which has projected all deformation onto the fault plane. Accordingly, future work should focus on clarifying the roles of each slab in the observed unstable period, with the inclusion of processes additional to elastic dislocation.

This sudden extension in the slab before the Tohoku-oki earthquake that we describe in this work was previously reported in a study of satellite gravity measurements[47], although the statistical significance of the reported gravity gradient anomaly is disputed[48]. This anomalous gravity-gradient signal begins a month later than the onset of extension recorded by GNSS in our study. Assuming that the reported gravity-gradient anomaly is valid, then a delay of just one month in these observations would indicate that these independent measurements are capturing the same process. The discrepancy in onset could also be reduced if we consider monthly sampling of the gravity data. The favoured extension model for the gravity gradient signal is a deep normal faulting in the Pacific Plate at depths greater than 245 km, whereas our modelling suggests that extension (the hinge line between apparent enhanced slip and locking) is shallower, at depths of approximately 50–100 km and with the extension signal starting in the Philippine Sea Plate.

Compared to the pre-Tohoku-oki case, prior to the Maule earthquake there were far fewer GNSS stations and much higher variability in station spacing. Therefore, elastic dislocation modelling for the Maule unstable period was not carried out. Nevertheless, owing to the reversing nature of the pre-Maule signal, we suspect that a sequence of events consisting of deeper slab pull interacting with bursts of slow slip further updip—similar to what occurred before the Tohoku-oki earthquake—also occurred before the Maule earthquake (see discussion in the Methods).

A spectrum of interseismic processes

In conclusion, we have identified enhanced slab pulling as the likely driving mechanism for the wobbles observed before the Tohoku-oki and Maule earthquakes. However, had the asperities updip of the pulling not been mature, it is conceivable that the unstable periods caused by enhanced slab pulling would have ceased without any great earthquake occurring. Likewise, we suggest that overdue (mature) earthquake segments might only tend to rupture after receiving sufficient additional shear stress from an acceleration in deeper subduction. In this context, the earthquake research community should be considering the frictional conditions of the seismogenic plate interface in

conjunction with the variable boundary conditions that seem to have a role in bringing large mature segments to failure.

Comparing the timing of the unstable phase reported in our study to the reported foreshock activity of other studies is not straightforward, owing to considerations of seismic network resolution and varied waveform processing strategies. Although there is anomalous seismicity identified before the Tohoku-oki and Maule earthquakes on the timescale of one to a few months before the mainshock, most of this analysis has been focused closer to the mainshock location. The large wobbles reported in our study appear to be mainly aseismic and affect far-field regions larger than the extent of the rupture zone on the subduction plate interface. It is worth noting here that the adjective 'aseismic' is defined by the threshold for which events can be detected with existing seismological networks. This threshold can be limited both by seismic processing strategies and network geometry. Therefore, there may be some as-yet-undetected seismic signals either along the plate interface or deeper inside the slab that correlate with these large-scale anomalous GNSS recorded motions.

Finally, we have focused on describing the most striking transient tectonic motions that we observe before the Maule and Tohoku-oki earthquakes. There are, however, many other tectonically intriguing signals in the periods analysed (Supplementary Videos 3 and 5), some of which could be related to other, smaller-magnitude earthquakes. Although we are able to notice large, tectonically driven wobbles of the surface before the Maule and Tohoku-oki earthquakes, we still do not know how prevalent these wobbles are at plate boundary zones worldwide, whether they scale according to subsequent earthquake magnitude, and therefore whether or not they can be used as reliable precursors for the imminence of major earthquakes. What is clear from this study is that subduction zones are highly dynamic on the human observable timescale and that whereas some transient events are apparent on the thousand-kilometre scale, others are very localized. To improve our understanding of the interaction of boundary conditions on relatively smaller potential rupture zones it will be essential to harness the growing amounts of GNSS data[49] to investigate the interaction of tectonic systems on the continental scale.

Online content

Any methods, additional references, Nature Research reporting summaries, source data, extended data, supplementary information, acknowledgements, peer review information; details of author contributions and competing interests; and statements of data and code availability are available at https://doi.org/10.1038/s41586-020-2212-1.

1. Kajitani, Y., Chang, S. E. & Tatano, H. Economic impacts of the 2011 Tohoku-Oki earthquake and tsunami. *Earthq. Spectra* **29**, 457–478 (2013).
2. Sagiya, T., Miyazaki, S. I. & Tada, T. Continuous GPS array and present-day crustal deformation of Japan. *Pure Appl. Geophys.* **157**, 2303–2322 (2000).
3. Báez, J. C. et al. The Chilean GNSS network: current status and progress toward early warning applications. *Seismol. Res. Lett.* **89**, 1546–1554 (2018).
4. Heki, K. & Mitsui, Y. Accelerated Pacific plate subduction following interplate thrust earthquakes at the Japan trench. *Earth Planet. Sci. Lett.* **363**, 44–49 (2013).
5. Loveless, J. P. & Meade, B. J. Two decades of spatiotemporal variations in subduction zone coupling offshore Japan. *Earth Planet. Sci. Lett.* **436**, 19–30 (2016).
6. Melnick, D. et al. The super-interseismic phase of the megathrust earthquake cycle in Chile. *Geophys. Res. Lett.* **44**, 784–791 (2017).
7. Bedford, J. & Bevis, M. Greedy automatic signal decomposition and its application to daily GPS time series. *J. Geophys. Res. Solid Earth* **123**, 6992–7003 (2018).
8. Reid, H. F. *The Mechanics of the Earthquake, The California Earthquake of April 18, 1906, Report of the State Investigation Commission* Vol. 2, 16–28 (Carnegie Institution of Washington, 1910).
9. Schurr, B. et al. Gradual unlocking of plate boundary controlled initiation of the 2014 Iquique earthquake. *Nature* **512**, 299–302 (2014).
10. Mavrommatis, A. P., Segall, P. & Johnson, K. M. A decadal-scale deformation transient prior to the 2011 Mw 9.0 Tohoku-oki earthquake. *Geophys. Res. Lett.* **41**, 4486–4494 (2014).
11. Wang, K. et al. Learning from crustal deformation associated with the M9 2011 Tohoku-oki earthquake. *Geosphere* **14**, 552–571 (2018).
12. Kato, A. et al. Propagation of slow slip leading up to the 2011 Mw 9.0 Tohoku-Oki earthquake. *Science* **335**, 705–708 (2012).
13. Johnson, P. A. et al. Acoustic emission and microslip precursors to stick-slip failure in sheared granular material. *Geophys. Res. Lett.* **40**, 5627–5631 (2013).
14. Kaproth, B. M. & Marone, C. Slow earthquakes, preseismic velocity changes, and the origin of slow frictional stick-slip. *Science* **341**, 1229–1232 (2013).
15. Lohman, R. B. & Murray, J. R. The SCEC geodetic transient detection validation exercise. *Seismol. Res. Lett.* **84**, 419–425 (2013).
16. Dill, R. & Dobslaw, H. Numerical simulations of global-scale high-resolution hydrological crustal deformations. *J. Geophys. Res. Solid Earth* **118**, 5008–5017 (2013).
17. van Dam, T. et al. Crustal displacements due to continental water loading. *Geophys. Res. Lett.* **28**, 651–654 (2001).
18. Heki, K. Snow load and seasonal variation of earthquake occurrence in Japan. *Earth Planet. Sci. Lett.* **207**, 159–164 (2003).
19. Wdowinski, S., Bock, Y., Zhang, J., Fang, P. & Genrich, J. Southern California permanent GPS geodetic array: spatial filtering of daily positions for estimating coseismic and postseismic displacements induced by the 1992 Landers earthquake. *J. Geophys. Res. Solid Earth* **102**, 18057–18070 (1997).
20. Bouchon, M. et al. Potential slab deformation and plunge prior to the Tohoku, Iquique and Maule earthquakes. *Nat. Geosci.* **9**, 380–383 (2016).
21. Gardonio, B. et al. Seismic activity preceding the 2011 M w 9.0 Tohoku earthquake, Japan, analyzed with multidimensional template matching. *J. Geophys. Res. Solid Earth* **124**, 6815–6831 (2019).
22. Ito, Y. et al. Episodic slow slip events in the Japan subduction zone before the 2011 Tohoku-Oki earthquake. *Tectonophysics* **600**, 14–26 (2013).
23. Ito, Y., Hino, R., Suzuki, S. & Kaneda, Y. Episodic tremor and slip near the Japan Trench prior to the 2011 Tohoku-Oki earthquake. *Geophys. Res. Lett.* **42**, 1725–1731 (2015).
24. Katakami, S. et al. Spatiotemporal variation of tectonic tremor activity before the Tohoku-Oki earthquake. *J. Geophys. Res. Solid Earth* **123**, 9676–9688 (2018).
25. Becker, T. W., Hashima, A., Freed, A. M. & Sato, H. Stress change before and after the 2011 M9 Tohoku-oki earthquake. *Earth Planet. Sci. Lett.* **504**, 174–184 (2018).
26. Yokota, Y. & Koketsu, K. A very long-term transient event preceding the 2011 Tohoku earthquake. *Nat. Commun.* **6**, 5934 (2015).
27. Pollitz, F. F. Coseismic deformation from earthquake faulting on a layered spherical Earth. *Geophys. J. Int.* **125**, 1–14 (1996).
28. Hayes, G. P. et al. Slab2, a comprehensive subduction zone geometry model. *Science* **362**, 58–61 (2018).
29. Rogers, G. & Dragert, H. Episodic tremor and slip on the Cascadia subduction zone: the chatter of silent slip. *Science* **300**, 1942–1943 (2003).
30. Yamashita, Y. et al. Migrating tremor off southern Kyushu as evidence for slow slip of a shallow subduction interface. *Science* **348**, 676–679 (2015).
31. Ide, S., Beroza, G. C., Shelly, D. R. & Uchide, T. A scaling law for slow earthquakes. *Nature* **447**, 76–79 (2007).
32. Savage, J. C. A dislocation model of strain accumulation and release at a subduction zone. *J. Geophys. Res. Solid Earth* **88**, 4984–4996 (1983).
33. Kodaira, S. et al. High pore fluid pressure may cause silent slip in the Nankai Trough. *Science* **304**, 1295–1298 (2004).
34. Tsuji, Y., Nakajima, J. & Hasegawa, A. Tomographic evidence for hydrated oceanic crust of the Pacific slab beneath northeastern Japan: implications for water transportation in subduction zones. *Geophys. Res. Lett.* **35**, L14308 (2008).
35. Liu, X., Zhao, D. & Li, S. Seismic attenuation tomography of the Northeast Japan arc: insight into the 2011 Tohoku earthquake (Mw 9.0) and subduction dynamics. *J. Geophys. Res. Solid Earth* **119**, 1094–1118 (2014).
36. Taetz, S., John, T., Bröcker, M., Spandler, C. & Stracke, A. Fast intraslab fluid-flow events linked to pulses of high pore fluid pressure at the subducted plate interface. *Earth Planet. Sci. Lett.* **482**, 33–43 (2018).
37. Ujiie, K. Chemical origin of tectonic tremor. *Nat. Geosci.* **12**, 962–963 (2019).
38. Incel, S. et al. Reaction-induced embrittlement of the lower continental crust. *Geology* **47**, 235–238 (2019).
39. Austrheim, H. Eclogitization of lower crustal granulites by fluid migration through shear zones. *Earth Planet. Sci. Lett.* **81**, 221–232 (1987).
40. John, T. & Schenk, V. Partial eclogitisation of gabbroic rocks in a late Precambrian subduction zone (Zambia): prograde metamorphism triggered by fluid infiltration. *Contrib. Mineral. Petrol.* **146**, 174–191 (2003).
41. Seno, T. & Maruyama, S. Paleogeographic reconstruction and origin of the Philippine Sea. *Tectonophysics* **102**, 53–84 (1984).
42. Bach, W. & Früh-Green, G. L. Alteration of the oceanic lithosphere and implications for seafloor processes. *Elements* **6**, 173–178 (2010).
43. Burnley, P. C., Green, H. W. & Prior, D. J. Faulting associated with the olivine to spinel transformation in Mg_2GeO_4 and its implications for deep-focus earthquakes. *J. Geophys. Res. Solid Earth* **96**, 425–443 (1991).
44. Thielmann, M., Rozel, A., Kaus, B. J. P. & Ricard, Y. Intermediate-depth earthquake generation and shear zone formation caused by grain size reduction and shear heating. *Geology* **43**, 791–794 (2015).
45. Fukao, Y. & Obayashi, M. Subducted slabs stagnant above, penetrating through, and trapped below the 660 km discontinuity. *J. Geophys. Res. Solid Earth* **118**, 5920–5938 (2013).
46. Kawakatsu, H. & Yoshioka, S. Metastable olivine wedge and deep dry cold slab beneath southwest Japan. *Earth Planet. Sci. Lett.* **303**, 1–10 (2011).
47. Panet, I., Bonvalot, S., Narteau, C., Remy, D. & Lemoine, J. M. Migrating pattern of deformation prior to the Tohoku-Oki earthquake revealed by GRACE data. *Nat. Geosci.* **11**, 367–373 (2018).
48. Wang, L. & Burgmann, R. Statistical significance of precursory gravity changes before the 2011 M_w 9.0 Tohoku-Oki earthquake. *Geophys. Res. Lett.* **46**, 7323–7332 (2019).
49. Blewitt, G., Hammond, W. C. & Kreemer, C. Harnessing the GPS data explosion for interdisciplinary science. *Eos* **99**, https://doi.org/10.1029/2018EO104623 (2018).

Methods

GNSS time series

For the South American network, all GNSS data were organized in units of 24-h periods and were processed using the Earth Parameter and Orbit System software (EPOS)[50]. The data processing was done in three steps. In the first step, all the stations were processed in a precise point positioning (PPP) model using the GNSS satellite clock and orbit products of the GFZ German Research Centre for Geosciences[51]. During PPP processing, bad observations and outliers were removed. In the second step, we followed a network-processing strategy based upon the PPP solutions and remaining observations. Up to 56 well distributed International GNSS Service (IGS) core stations are included in the network. Since the number of project stations can reach up to about 800, and the Earth Parameter and Orbit System software can process up to 250 stations for one single network, the project stations were processed in several sub-networks. Depending on data availability, ten well distributed IGS stations were included in each sub-network to connect all the sub-networks. In the network processing, all the stations were treated with the same weight. Since we did not fix any station in the network processing, the coordinate solution is the same as a free network solution. The datum of the coordinate solution was defined by the satellite orbit and clock products used in the 2008 realization of the International Terrestrial Reference Frame (ITRF2008; http://itrf.ensg.ign.fr/). In the third and final step, the network solution was aligned to the IGS second reprocessing combined daily coordinate product in ITRF2014[52,53] to reduce the impact of the datum effect. To avoid the artefacts caused by reference stations, the IGS second solutions were visually inspected. Those IGS station time series that show transient signals in the unstable period defined in this study were not used for the alignment. The coordinate results from the network solution have an accuracy of a few millimetres. IGS stations used in the network data processing are indicated in Extended Data Fig. 1.

For the Japanese case, we use coordinates from the network solutions (version F3), provided by the Geospatial Information Authority of Japan[54].

GNSS data postprocessing for the pre-Maule-earthquake solutions

We considered time series between 1 January 2005 and 25 February 2010. Time series were retained if they had a minimum of four years of data and also spanned the year preceding the Maule earthquake. Obvious, grossly outlying points were removed from the network solutions by manual inspection. Likewise, any very large artificial steps were removed. Data were further de-spiked by the application of a median filter and removal of points far from this filtered trace. We note that the median filter is only used for outlier detection and the unfiltered series, with outliers removed, is fed into the GrAtSiD algorithm.

GNSS data postprocessing for the pre-Tohoku-oki-earthquake solutions

Time series were truncated between 1 January 2006 and 8 March 2011. Time series were retained if they had a minimum of four years of data and also spanned the year preceding the Tohoku-oki earthquake. Data were provided in degrees and so these were converted into metres. Next, the median filter approach for outlier removal (as done for South American data) was applied.

Signal decomposition with GrAtSiD

The post-processing procedure described in this section was applied to both the pre-Maule and pre-Tohoku datasets. For each directional component (East, North and Up) of each GNSS station, we applied an initial GrAtSiD fit[7] with one convergence only. GrAtSiD is a greedy linear regression routine that aims to find a minimum number of transient (multi-transient) and step (Heaviside) basis functions present in the time series. In general, greedy algorithms sequentially test for the improvement of fit when including additional basis functions in the model[55]. Basis functions that are always present in the GrAtSiD solution (permanent functions) are the Fourier functions for annual and semi-annual oscillations, the first-order polynomial terms (linear trend and constant shift), and the steps imposed owing to known hardware changes or when the station is within a radial cut-off distance from a catalogued earthquake, with the cut-off distance r (in kilometres), being $r = 10^{0.5M-0.8}$, where M is the earthquake magnitude (as also used by the Nevada Geodetic Laboratory[49]). For the Maule data, we considered all events with at least magnitude 5, as provided by the catalogue of the National Earthquake Information Center of the United States Geological Survey (USGS NEIC) (https://earthquake.usgs.gov/earthquakes/search/), whereas for the Tohoku-oki data we considered moment magnitudes ≥6, again taken from the USGS NEIC catalogue. Permanent functions also include the known times of steps due to equipment- or processing-related discontinuities.

The regression model, $x(t)$, of GrAtSiD is formulated as follows:

$$x(t) = mt + d + \sum_{k=1}^{n_k} [s_k \sin(\omega_k t) + s_k \cos(\omega_k t)] + \sum_{j=1}^{n_j} b_j H(t - t_j) + \sum_{r=1}^{n_r} \sum_{i=1}^{n_i} [A_i (1 - e^{-(t-t_r)/T_i})] + \xi(t)$$

in which t is time, and m and d are the coefficients of the first-order polynomial. The sine and cosine functions model the annual and semi-annual background seasonal oscillations in the signals with $n_k = 2$ (coefficients s_k and c_k). $H(t - t_j)$ represent the Heaviside functions that are pre-defined as basis functions or automatically found with GrAtSiD (with b_j being the coefficients for events at time t_j). The double summation term represents the r multi-transients, which are the sum of exponential functions starting at t_r. T_i are the decay constants and we use three for each multi-transient. A multi-transient is a decaying function that is made from the sum of multiple decay functions—in this case we implement exponential decay functions but we could also use logarithmic decays. By not constraining the signs of coefficients (A_i), we can produce, with one or two multi-transients in series, a variety of signal shapes. Accordingly, the multi-transient is chosen as a sparse basis function in the regression because it is a versatile function that can capture transient signals of varying durations. $\xi(t)$ is the residual. The above equation looks very similar to the Extended Linear Trajectory Model (ELTM) described in equation (10) of ref. [56] except that the transient functions (single transients) are replaced with multi-transients. Full details of the algorithm can be found in the GrAtSiD methods paper[7] along with videos that illustrate the convergence of the solution for multiple examples.

The purpose of the initial GrAtSiD fit is to estimate a residual time series for each component of each station. Using the common-mode error reduction approach[19], we then took the median residual value for each directional component (as a function of time) and subtracted this from the corresponding time series. Next, we applied GrAtSiD again on the common-mode corrected time series. The common-mode filter also serves as a low-pass filter and is effective in removing high-frequency noise such as reference frame jitter[56] as well as reducing heteroskedasticity in the network solutions. Five convergences were run for each time series of the Japanese F3 solutions and 30 were run for the pre-Maule-earthquake time series. The solution that is most similar to other convergences was chosen as the solution for the decomposition. Similarity is defined by the solution that has the smallest average residual to all other solutions[7]. For Fig. 3, Extended Data Fig. 4, and Supplementary Videos 3–8, the seasonal contributions and the steps in the GrAtSiD trajectories were removed: that is, the Fourier functions and Heaviside functions (that have been imposed from seismic catalogues or automatically found with GrAtSiD), are removed from the solution

(simply done by removing these terms from the linear combination of basis functions).

Extended Data Figs. 2 and 3 show example results of the signal decomposition and how time series are cleaned by the removal of background seasonal oscillation and common-mode noise (see also Supplementary Videos 1 and 2). Extended Data Fig. 4 shows the velocity table for all three directional components in Japan (as shown in the East component only in Fig. 3a) while the Source Data for Fig. 3 gives the non-overlapping along-strike rectangular regions used in this analysis. Extended Data Fig. 5 shows the effect of removing modelled terms from the trajectory model that was optimized by GrAtSiD.

Investigating possible non-tectonic sources of the transient signal

The following sub sections describe the tests done to determine whether the unstable periods before the Maule and Tohoku-oki earthquakes, defined in this study by times where we observe the strong transient motions in the GNSS time series, are likely to be non-tectonic in origin. Possible non-tectonic sources that we investigate include: (1) artefacts from GNSS processing, such as systematic and sustained distortion of the reference frame over large distances, and (2) unusually strong interannual variations in seasonal fluid loading of the Earth's surface (oceanic, atmospheric and hydrological) that would be decomposed into the non-seasonal portion of the signal by the GrAtSiD algorithm (GrAtSiD assumes a steady background oscillation described by annual and semi-annual Fourier functions).

Investigation of possible processing-related artefacts. As stated above, for both sets of time series, we applied a common-mode filter that removes much of the higher-frequency reference frame jitter in the network solution. To reduce the chance of having large lower-frequency distortions of the reference frame (which can appear to be tectonic transients in the region of interest) one must exclude any stations that cannot be well modelled by the assumed trajectory model from the list of stations used to define the reference frame[56]. For the pre-Maule-earthquake analysis, we followed a careful selection of reference stations that are largely free of artefacts and, furthermore, we selected stations far away from the regions suspected to be strongly affected by tectonic transient motion. As an additional test, we split our analysed time series into two groups: group 1 we deem to be affected by the unstable period and group 2 we deem to be unaffected. Extended Data Fig. 6 shows a map and median variation in detrended velocity in each directional component for both groups. We can see that the strong east–west wobbling is most pronounced in stations that are not used in defining the reference frame and in regions where we are interpreting the pre-Maule unstable transient period to be manifest. There is a hint of some of the transient signal of group 2 in the North and Vertical component correlating with the Group 1 East component, although this analysis is hindered by the relative lack of stations in regions far away from the suspected transient-affected region. Furthermore, it can be observed in Supplementary Videos 5 and 6 that the wobble of the unstable period in the East–West direction is strongest along the Group 1 stations. The observation that the East–West unstable period transient motion is not as pronounced in Group 2 points towards the observed transient in Group 1 being largely unrelated to processing artefacts.

One notable feature of the pre-Tohoku-oki wobble that cannot be easily explained by a reference frame problem is the propagation of the wobble signal (as shown in Fig. 3a, b). Still, for the Tohoku-oki earthquake we wanted to perform an analysis similar to that done for the Maule earthquake, in which we look for the spatial extents of the wobbling signal. For the Japanese F3 network solutions, we are not able to replicate such an analysis because the whole of the network seems to be affected during the unstable period. Therefore, we took IGS08 (the 2008 datum of the IGS) PPP solutions[57,58] from the Nevada Geodetic Laboratory[49] for stations spanning a wider spatial extent on the globe. The signal decomposition is as described above (that is, outlier removal and application of GrAtSiD for signal decomposition) but without the application of a common-mode filter (since high-frequency noise in the PPP solutions correlates less on the daily scale compared to network solutions). Extended Data Fig. 7 shows the extent of the network with group 1 (affected stations) and group 2 (largely unaffected stations) with the median variation in detrended velocity of each directional component for both groups. From Extended Data Fig. 7 and the video of the unstable period for this larger-spatial-scale dataset (Supplementary Video 8) we can see that the affected region spans into the Korean Peninsula, China, Russia, and elsewhere, with a hint of extension between Japan and the Korean Peninsula and Russia. Much further away, we see that there is minimal variation in the detrended velocities during this unstable period (Supplementary Video 8).

A direct comparison of the Nevada Geodetic Laboratory (NGL)'s PPP and the Geospatial Information Authority of Japan (GSI)'s F3 solutions can be seen in Extended Data Fig. 8. Here we see that the wobble of the unstable period is apparent in both sets of solutions. From this analysis of the GNSS time series before the Tohoku-oki earthquake, we conclude that the transient of the unstable period is most probably not an artefact of GNSS processing. Furthermore, from both velocity analysis of modelled trajectories and visual comparisons of daily solutions we see the same duration and motions of the unstable period for the East component, both in the PPP and network F3 solutions. In the North and Vertical components of the PPP, we do not see the unstable period in group 1 as clearly as we do for the F3 solutions. This is partially due to the daily repeatability noise being larger in the PPP solutions.

Investigation into interannual variations in fluid loading. It is well established that hydrological, oceanic and atmospheric loading controls the seasonal oscillation observed in GNSS time series[17,59]. Accordingly, highly anomalous changes in the amount of fluid loading can greatly affect the amplitude of the oscillation of a particular season[60], whereas longer changes (for example, Earth's current rapid climate change) can manifest themselves as noticeable changes in the background trend of GNSS time series[61,62], particularly in the vertical component of motion. One simplifying assumption of the GrAtSiD algorithm is that there exists a constant background seasonal oscillation that is modelled as the sum of annual-period and semi-annual-period sine and cosine functions. Accordingly, GrAtSiD will map any strongly anomalous (unseasonal) fluid-loading-induced motion into the sparse portion of the signal that comprises multi-transient functions[7]. Such an assumption, however, is workable when we do not anticipate too much anomalous seasonal motion in the time series. Given the constraints in the assumptions of the GrAtSiD algorithm, we performed an additional investigation into whether the fluid loading (caused by precipitation, and by oceanic and atmospheric loading) could be a strong candidate to explain the unstable period motion before the Maule and Tohoku-oki earthquakes.

At all GNSS station locations, we gathered predictions of displacement due to fluid loading and decomposed these into annual and interannual surface displacements using GrAtSiD. The predictions for surface displacements are a sum of predictions provided by the GeoForschungsZentrum Potsdam Earth-System-Modelling (http://esmdata.gfz-potsdam.de:8080/repository)[16]. We summed the predictions of non-tidal atmospheric loading, non-tidal oceanic loading, hydrological loading and barystatic sea-level loading (NTAL + NTOL + HYDL + SLEL) to produce daily time series of predicted GNSS displacement in the same three directional components as the GNSS time series. All of these prediction products are generated by convolving fluid loading measurements with Green's functions of Earth's elastic response[16].

For both GNSS measured and fluid predicted displacements we applied the same processing flow: first we ran GrAtSiD to fit a trajectory model to each time series. Next, we isolated the multi-transient and polynomial terms for each time series and generated velocity time series. From these velocity time series we subtracted the median velocity of the observation period to leave behind a time series measuring the

deviation from median velocity (the deviation from the 'steady-state' velocity at each station). Finally, we take the median of these median corrected velocities across all time series to produce a measure of the overall transient motion of the stations. This is the same approach as described above (Extended Data Figs. 6, 7 and Fig. 2c, f). For the Tohoku-oki and Maule earthquakes, respectively, Extended Data Figs. 9 and 10 show the maps and time series of stations used in the comparison of measured and predicted displacements for the Tohoku-oki and Maule earthquakes, respectively.

From comparing the predicted and observed velocities in Extended Data Figs. 9 and 10, we see that there is no strong agreement in the onset of the observed unstable phase and the predicted velocities. This is especially so in the East component in both pre-Maule and pre-Tohoku-oki data, for which the strongest explanation of this motion in this component remains tectonics. Perhaps the strongest indication that fluid loading might be involved in the observed unstable period can be seen in the Vertical component in Japan. In this case, the median predicted deviation of velocity of the network is relatively unstable compared to the previous period across the whole network from mid-2010 until the onset of the Tohoku-oki earthquake and, although both the polarity of motion and onset of the predicted and observed unstable phases are not in good agreement, it could be that the unusually strong fluctuations in fluid loading (visible in the Vertical prediction) have contributed to tipping a critically stressed subduction system into instability.

Elastic dislocation modelling of the pre-Tohoku-oki unstable phase

To aid in the interpretation of the surface signal of the unstable phase, we constructed a kinematic model in which the surface displacements are predicted using Green's functions of elastic dislocation on the subduction plate interface in a layered isotropic spherical Earth[27]. The major drawback of such modelling is in the assumption that all motion can be related to plate interface kinematics in a purely elastic medium, whereas a more realistic (but harder to model) scenario includes processes such as viscoelastic and viscoplastic deformation.

From the Slab2 subduction interface geometry[28] we constructed 1,151 rectangular patches from which the Green's functions for elastic dislocation were calculated using the default Earth layering parameter file of the Static-1D software (https://github.com/fpollitz-usgs/STATIC1D)[27]. We used the convex optimization software CVXOPT[63] to solve for the updip dislocation value, m in the following problem: minimize$\{||d - Gm|| + \lambda||m||\}$, where d are the surface displacements, G is the matrix of Green's functions containing the surface predictions for unitary updip dislocations on each patch, and λ is the damping factor to regularize the inversion. We allowed the solution to find both negative and positive updip dislocation values, whereby negative values indicate transient enhanced locking[32] and positive values indicate transient slip. This freedom is given to the model because the nature of the signal (wobbling in East–West and Vertical directions) possibly indicates that there were periods of both enhanced slip and locking in this unstable phase. Furthermore, previous studies have allowed for the simultaneous presence of both enhanced locking and slip in kinematic models of the interseismic period[10,26]. The data have been interpolated onto a grid with squares of 2 decimal degrees, with each square containing at least ten stations and taking the median displacement from time series within each square, where each time series has been detrended from its median velocity. Figure 5 shows the results of the kinematic modelling at three separate points in time during the unstable phase. A separate model was made for the displacements of each day and these form the frames of Supplementary Video 7.

Interpretation of the pre-Maule unstable period signals

There are far fewer stations for the pre-Maule unstable period compared to the pre-Tohoku-oki unstable period. Nevertheless, given the similarity of the data features to those captured before the Tohoku-oki earthquake, we can hypothesize on the likely mechanisms at play. Whereas we do see some strong subsidence that could be indicative of enhanced slab pull, particularly in the back arc away from the Maule rupture zone and into Argentina, there is not a strong vertical reversal (as observed before the Tohoku-oki earthquake) and the wobbling that defines the unstable period is only clear in the East–West direction. Furthermore, there are insufficient stations to determine whether subsidence signal began with, before or after the East–West wobbling. Within the pre-Maule unstable period, there also does not appear to be a period of obvious extension. Therefore, we hypothesize that the simplest sequence of events starts with an increase in slab pull force causing a plunge (without any noticeable extension) of the downgoing slab and simultaneous eastwards motion as the locked shallower portion of the plate interface drags the continent at a higher-than-usual rate. This is followed by a large slow-slip event triggered by the increase in plate interface shear stress, which causes the overriding plate to move westwards. Fluids on this slab segment (which could facilitate the slow slip) have been inferred from tomography and are also thought to control longer-term subduction kinematics[64]. This slow slip is then arrested, while the faster velocity of the slab persists, resulting again in faster-than-usual westward motion. The next slow slip is either so close to the mainshock time that we do not resolve it before the mainshock, or it does not occur at all, with the enhanced shear stress on the plate interface causing the mainshock asperities to fail with minimal foreshock or foreslip activity. It is possible that the large slow slip that occurs during this sequence of events acts as the destabilizing event that enhances the slab pull. It is not clear how much of a viscoelastic component there is to the wobble signals recorded during the pre-Maule unstable period, although future modelling could tackle this question. The pull of the pre-Maule sequence seems to be coming from a very deep source: if we project vertically from the stations of strong subsidence down to the plate interface, we arrive at depths of several hundreds of kilometres, with depths of approximately 500 km estimated for the stations in Argentina[65], leading again to the interpretation of a buoyancy instability caused by a sudden transition of slab mantle material as it moves through a mantle transition zone.

Spatial averaging, time series detrending, and deviations from background velocity

In Fig. 3 and Extended Data Fig. 4, we plot the regional median deviation from background steady velocity, where the steady velocity of each station is first calculated by taking the median of the trend (minus seasonal and steps). Median velocity values are convenient to calculate owing to the smooth interseismic trends (the sum of the first-order polynomial and multi-transient functions) recovered from GrAtSiD. For each rectangular region, we calculate the median deviation from the background steady velocity (as a function of time) across each velocity time series in that region. Bounds for the non-overlapping regions are provided in the Source Data for Fig. 3 and Extended Data Fig. 4.

As done in Fig. 3 and Extended Data Fig. 4, we plot the median deviation in velocity from the background (also using median) velocity across groups of stations in Fig. 2c, f and Extended Data Figs. 6, 7, 9 and 10. Essentially, this allows us to generate measures of velocity that deviate from a steady state for particular directional components across groups of stations. As mentioned in the legend of Fig. 2, this average deviation from background velocity is only calculated if more than 55% of stations in the group have data on that particular day. This is to avoid spurious apparent deviations from velocity that arise from fewer samples.

For all Supplementary Videos 3–8 and for Figs. 3c and 4, the displacements are calculated from detrended time series, where the trend of the time series is determined by the median velocity of the smooth interseismic trends. Then within each regional window (for example, 2° by 2° for Supplementary Videos 3 and 4) the median detrended displacements are plotted in each frame.

Data availability

The daily GNSS displacement time series and the predicted displacements from fluid loading models are available in a data supplement to this paper[66].

Code availability

To create the maps in the figures and Supplementary videos, we used Python package Matplotlib[67] and Generic Mapping Tools[68]. The GrAtSiD code used for the trajectory modelling in this study can be provided upon request from the corresponding author.

50. Gendt, G. et al. *GFZ Analysis Center of IGS. Annual Report for 2013* 1–10 (GFZ German Research Centre for Geosciences, 2013); ftp://ftp.gfz-potsdam.de/GNSS/DOCS/IGS_repro2/GFZ_igs_annual_report_2013_iss1-0.pdf.
51. Deng, Z., Fritsche, M., Nischan, T. & Bradke, M. *Multi-GNSS Ultra Rapid Orbit-, Clock- & EOP-Product Series* (GFZ Data Services, 2016); https://doi.org/10.5880/GFZ.1.1.2016.003.
52. Rebischung, P., Altamimi, Z., Ray, J. & Garayt, B. The IGS contribution to ITRF2014. *J. Geodyn*. **90**, 611–630 (2016).
53. Altamimi, Z., Rebischung, P., Métivier, L. & Collilieux, X. ITRF2014: A new release of the International Terrestrial Reference Frame modeling nonlinear station motions. *J. Geophys. Res. Solid Earth* **121**, 6109–6131 (2016).
54. Nakagawa, H., et al. *Development and validation of GEONET New Analysis Strategy (Version 4) [in Japanese] Annual Report of the Geographical Survey Institute* Vol. 118, 1–8 (GSI, 2009); https://www.gsi.go.jp/common/000054716.pdf.
55. Needell, D., Tropp, J. & Vershynin, R. Greedy signal recovery review. In *2008 42nd Asilomar Conf. on Signals, Systems and Computers* 1048–1050, https://core.ac.uk/reader/23798095 (IEEE, 2008).
56. Bevis, M. & Brown, A. Trajectory models and reference frames for crustal motion geodesy. *J. Geod*. **88**, 283–311 (2014).
57. Rebischung, P. et al. IGS08: the IGS realization of ITRF2008. *GPS Solutions* **16**(4), 483–494 (2012).
58. Zumberge, J. F., Heflin, M. B., Jefferson, D. C., Watkins, M. M. & Webb, F. H. Precise point positioning for the efficient and robust analysis of GPS data from large networks. *J. Geophys. Res. Solid Earth* **102**, 5005–5017 (1997).
59. Liu, L., Khan, S. A., van Dam, T., Ma, J. H. Y. & Bevis, M. Annual variations in GPS-measured vertical displacements near Upernavik Isstrøm (Greenland) and contributions from surface mass loading. *J. Geophys. Res. Solid Earth* **122**, 677–691 (2017).
60. Kusche, J. E. J. O. & Schrama, E. J. O. Surface mass redistribution inversion from global GPS deformation and Gravity Recovery and Climate Experiment (GRACE) gravity data. *J. Geophys. Res. Solid Earth* **110**, B09409 (2005).
61. Borsa, A. A., Agnew, D. C. & Cayan, D. R. Ongoing drought-induced uplift in the western United States. *Science* **345**, 1587–1590 (2014).
62. Bevis, M. et al. Accelerating changes in ice mass within Greenland, and the ice sheet's sensitivity to atmospheric forcing. *Proc. Natl Acad. Sci. USA* **116**, 1934–1939 (2019).
63. Grant, M. & Boyd, S. CVX: Matlab software for disciplined convex programming. Version 2.1, http://cvxr.com/cvx/citing/ (2014).
64. Moreno, M. et al. Locking of the Chile subduction zone controlled by fluid pressure before the 2010 earthquake. *Nat. Geosci*. **7**, 292–296 (2014).
65. Chen, Y. W., Wu, J. & Suppe, J. Southward propagation of Nazca subduction along the Andes. *Nature* **565**, 441–447 (2019).
66. Bedford, J. et al. Trajectory models for daily displacement time series in the five years preceding the 2010 Maule Mw 8.8, Chile, and 2011 Tohoku-oki Mw 9.0, Japan earthquakes (GFZ Data Services, 2020); https://doi.org/10.5880/GFZ.4.1.2020.001.
67. Hunter, J. D. Matplotlib: a 2D graphics environment. *Comput. Sci. Eng*. **9**, 90–95 (2007).
68. Wessel, P., Smith, W. H., Scharroo, R., Luis, J. & Wobbe, F. Generic mapping tools: improved version released. *Eos* **94**, 409–410 (2013).

Acknowledgements We thank the Geospatial Information Authority of Japan (GSI) and the Nevada Geodetic Laboratory (NGL), University of Nevada, for their assistance and for providing time series for this study. We thank Y. Bock and K. Heki for comments. J.R.B. thanks S. Sobolev for his comments. J.R.B. thanks the German Science Foundation (DFG) for grant MO-2310/3. M.M. acknowledges support from FONDECYT 1181479, the Millennium Nucleus "The Seismic Cycle Along Subduction Zones" grant NC160025, and the Research Center for Integrated Disaster Risk Management (CIGIDEN), CONICYT/FONDAP 15110017. J.C.B. acknowledges support from FONDECYT projects 1170430 and 1181479.

Author contributions Z.D. and J.C.B. processed the South American network solutions. J.R.B., M.M. and B.S. performed postprocessing (analysis of daily GNSS time series). M.B., J.C.B., Z.D. and J.R.B. investigated the processing artefacts and non-tectonic signals. T.J., O.O. and J.R.B. performed the geophysical and geological interpretation. J.R.B. did the kinematic modelling. All authors assisted in editing the manuscript.

Competing interests The authors declare no competing interests.

Additional information
Supplementary information is available for this paper at https://doi.org/10.1038/s41586-020-2212-1.
Correspondence and requests for materials should be addressed to J.R.B.
Peer review information *Nature* thanks Yehuda Bock, Kosuke Heki and the other, anonymous, reviewer(s) for their contribution to the peer review of this work.
Reprints and permissions information is available at http://www.nature.com/reprints.

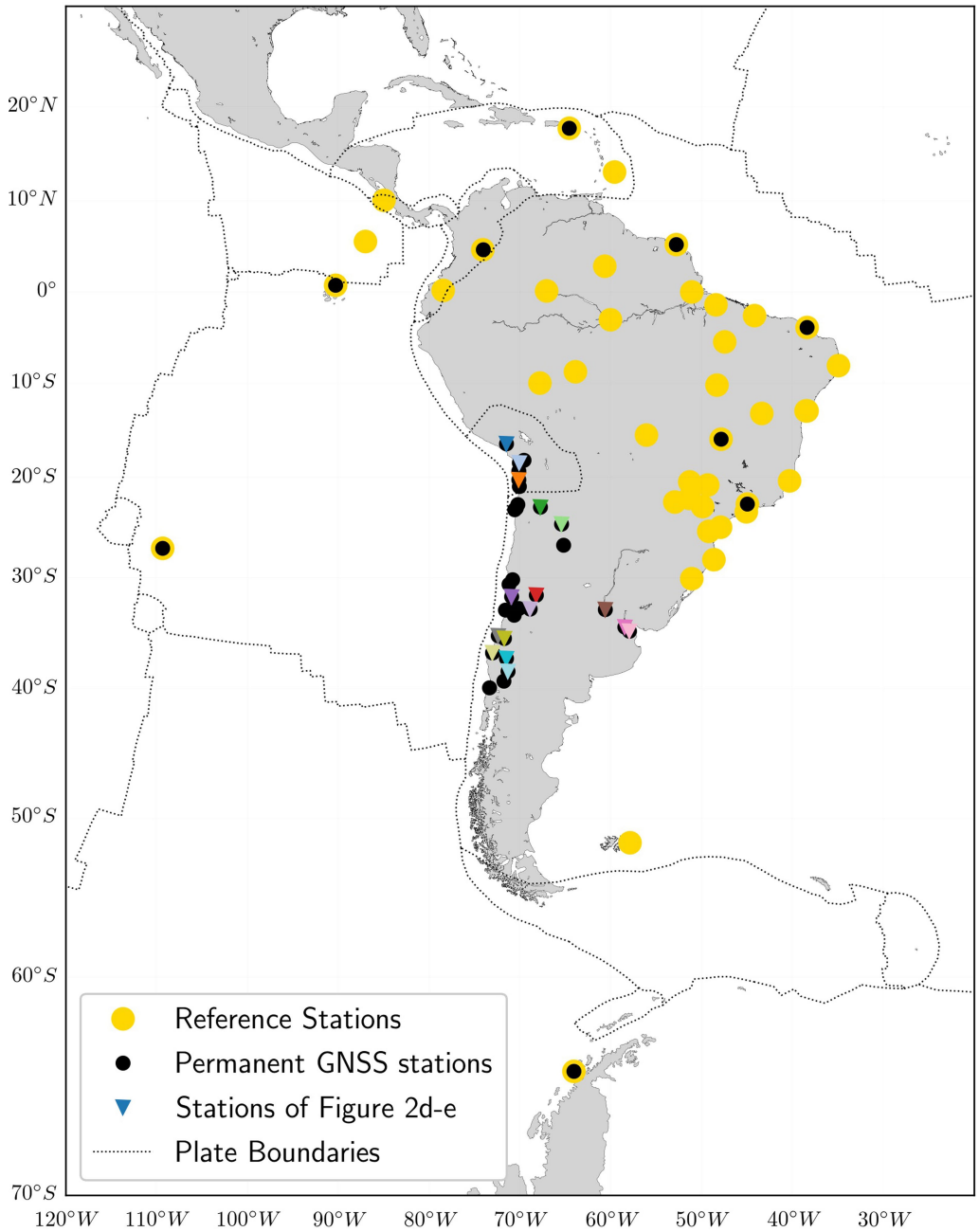

Extended Data Fig. 1 | Stations used in the processing and analysis of the pre-Maule-earthquake GNSS data. Locations of IGS stations used to define the reference frame of the network solutions are shown in gold. Black dots are the stations where network solutions are used in the time series analysis of the pre-Maule signals. Coloured triangles indicate locations of time series shown in Fig. 2 and Extended Data Fig. 3. There are some stations used to define the reference frame that are not used in the time series analysis owing to lack of data in the desired window (1 January 2005 until 25 February 2010).

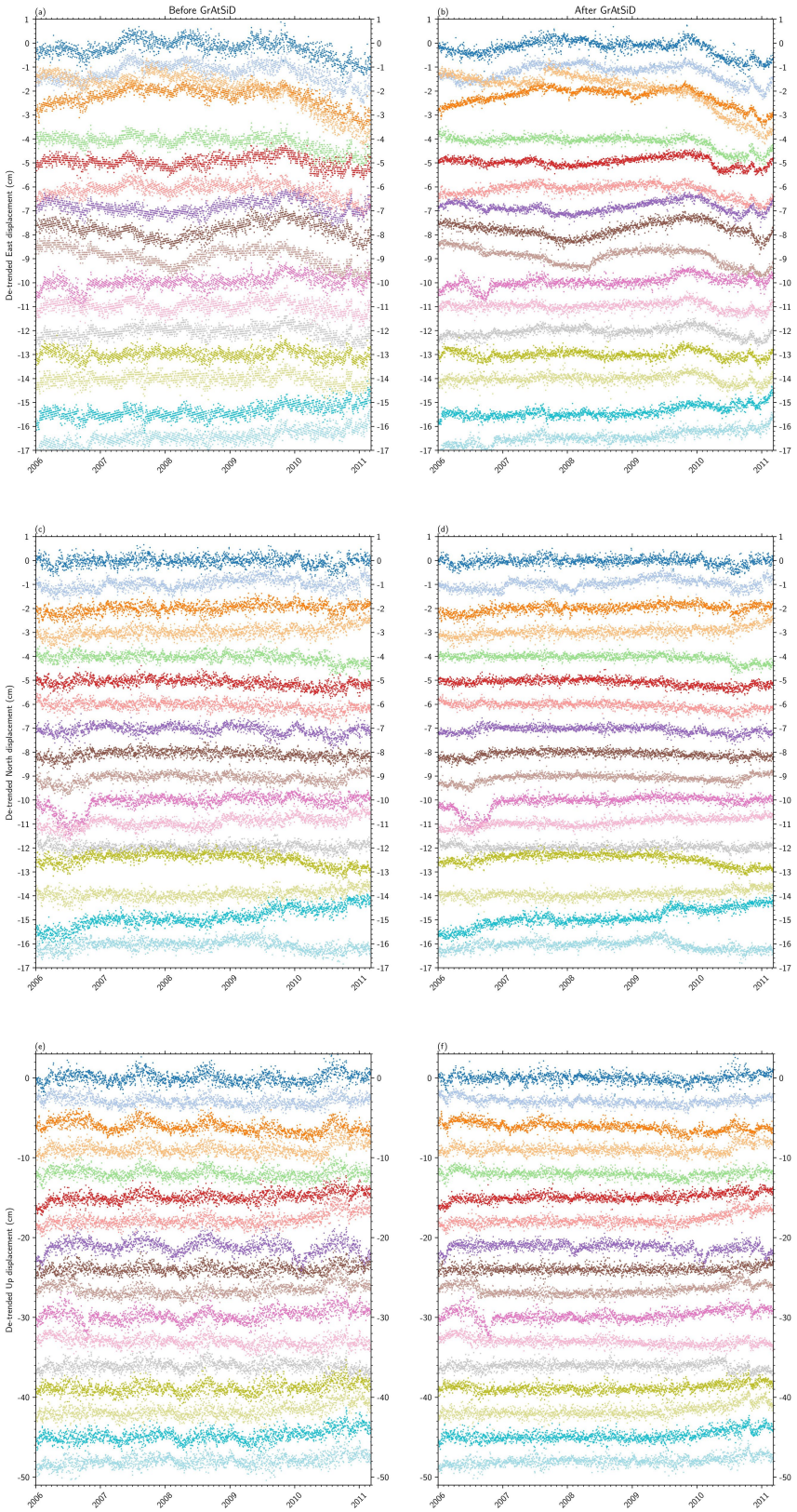

Extended Data Fig. 2 | Time series before the Tohoku-oki earthquake and the effect of noise removal with GrAtSiD in all three directional components. Left panels show the pre-Tohoku-oki F3 time series. Right panels show these time series after the removal of background seasonal and common-mode noise (with the GrAtSiD routine). The transient behaviour in the months before Tohoku-oki is heavily obscured by seasonal and common-mode noise. Colours correspond to locations on Fig. 1. For clarity, steps have been removed from all time series. Time series in these plots extend until three days before the mainshock.

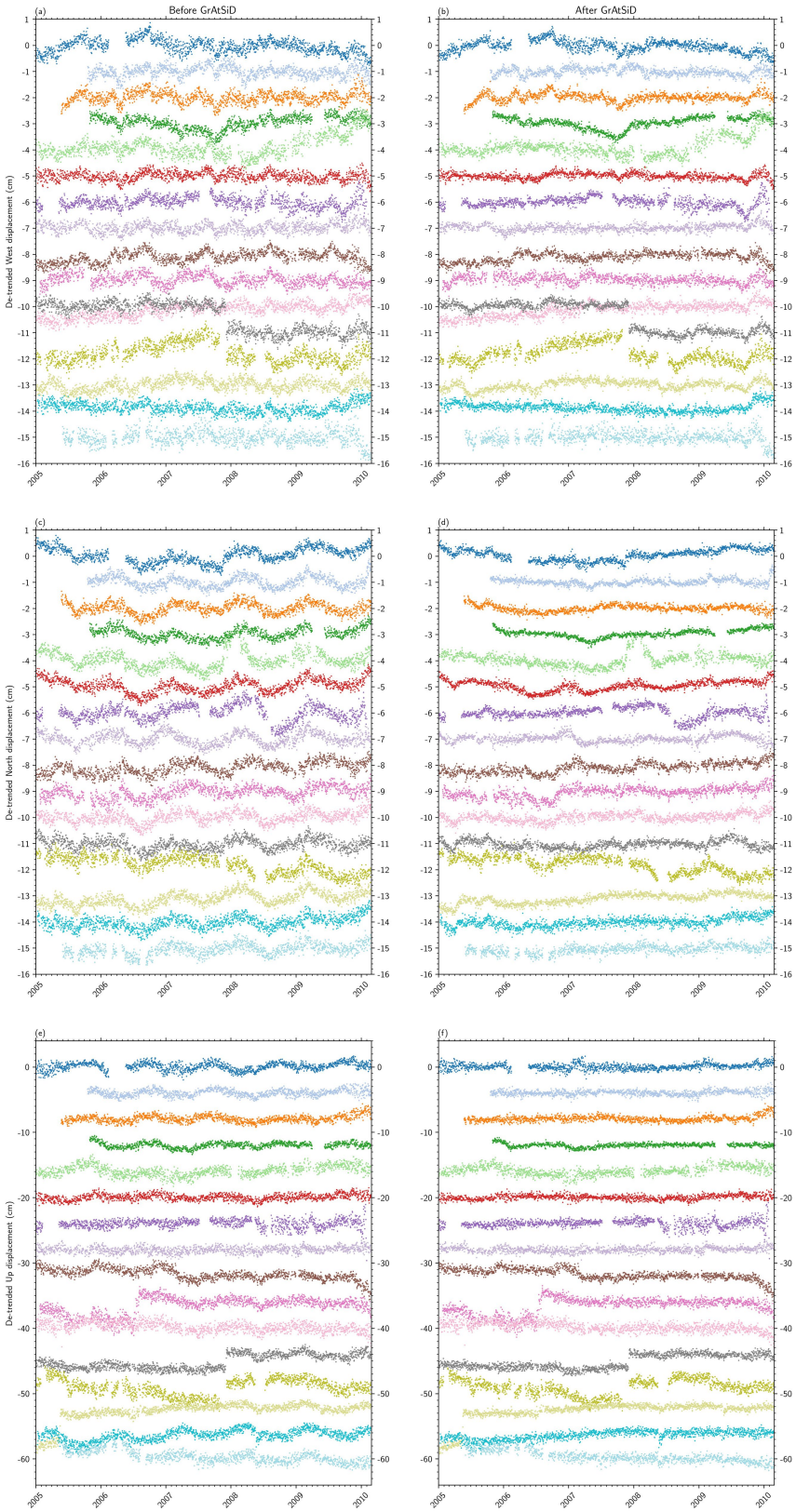

Extended Data Fig. 3 | Time series before the Maule earthquake and the effect of noise removal with GrAtSiD in all three directional components. Left panels show the pre-Maule time series. Right panels show these time series after the removal of background seasonal and common mode noise (with the GrAtSiD routine). The transient behaviour in the months before Maule event is heavily obscured by seasonal and common-mode noise. Colours correspond to locations on Fig. 1. For clarity, steps have been removed from all time series. Time series in these plots extend until two days before the mainshock.

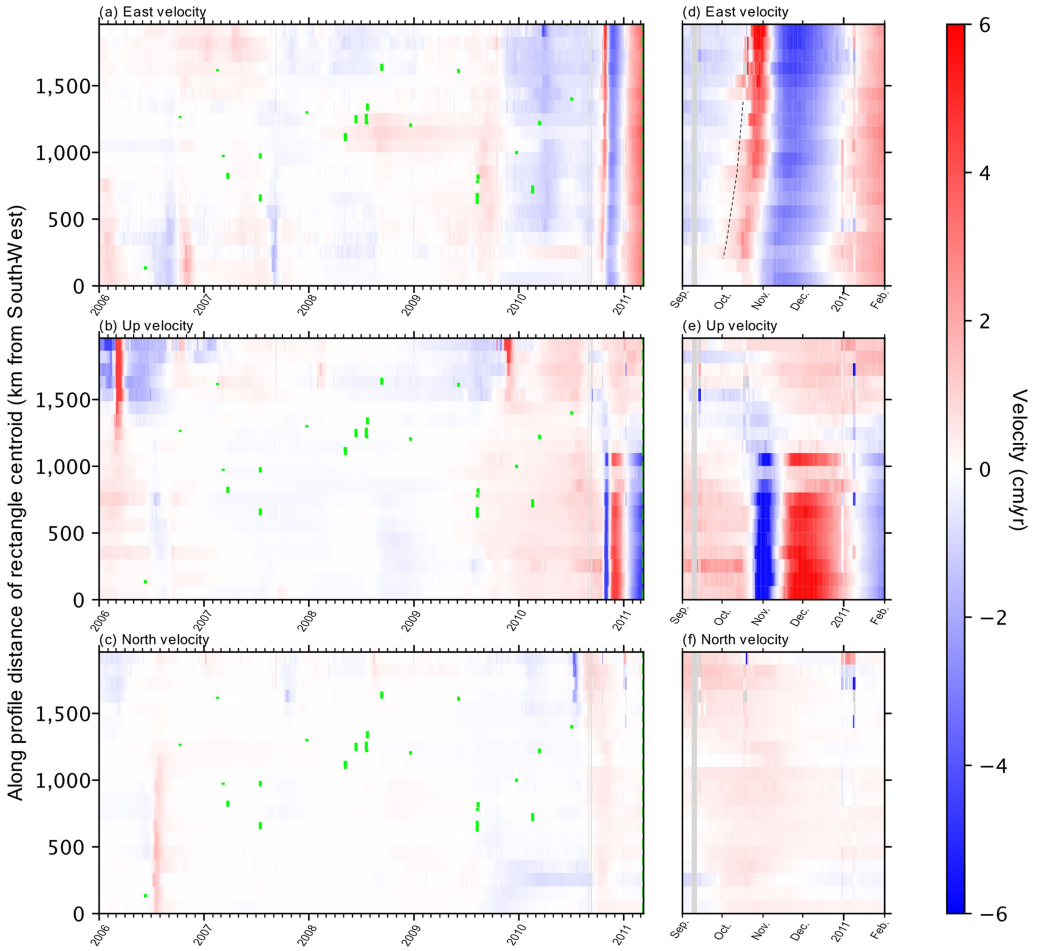

Extended Data Fig. 4 | Visualizing the along-strike signal migration and reversal of Japan in the years and months preceding the Tohoku-oki earthquake for all three directional components. Velocities within non-overlapping rectangular regions before the Tohoku-oki earthquake. The velocity for each region is detrended relative to the median velocity of that region between 1 January 2006 and 8 March 2011. Green lines indicate the along-strike locations and times of earthquakes of moment magnitude exceeding 6. Panels **d**–**f** are zoom-ins of panels **a**–**c** between the beginning of September 2010 and the beginning of February 2011. The dashed line on panel **d** indicates the velocity front that migrates across Japan from the southwest (shown in Supplementary Videos 3 and 4 and Fig. 3).

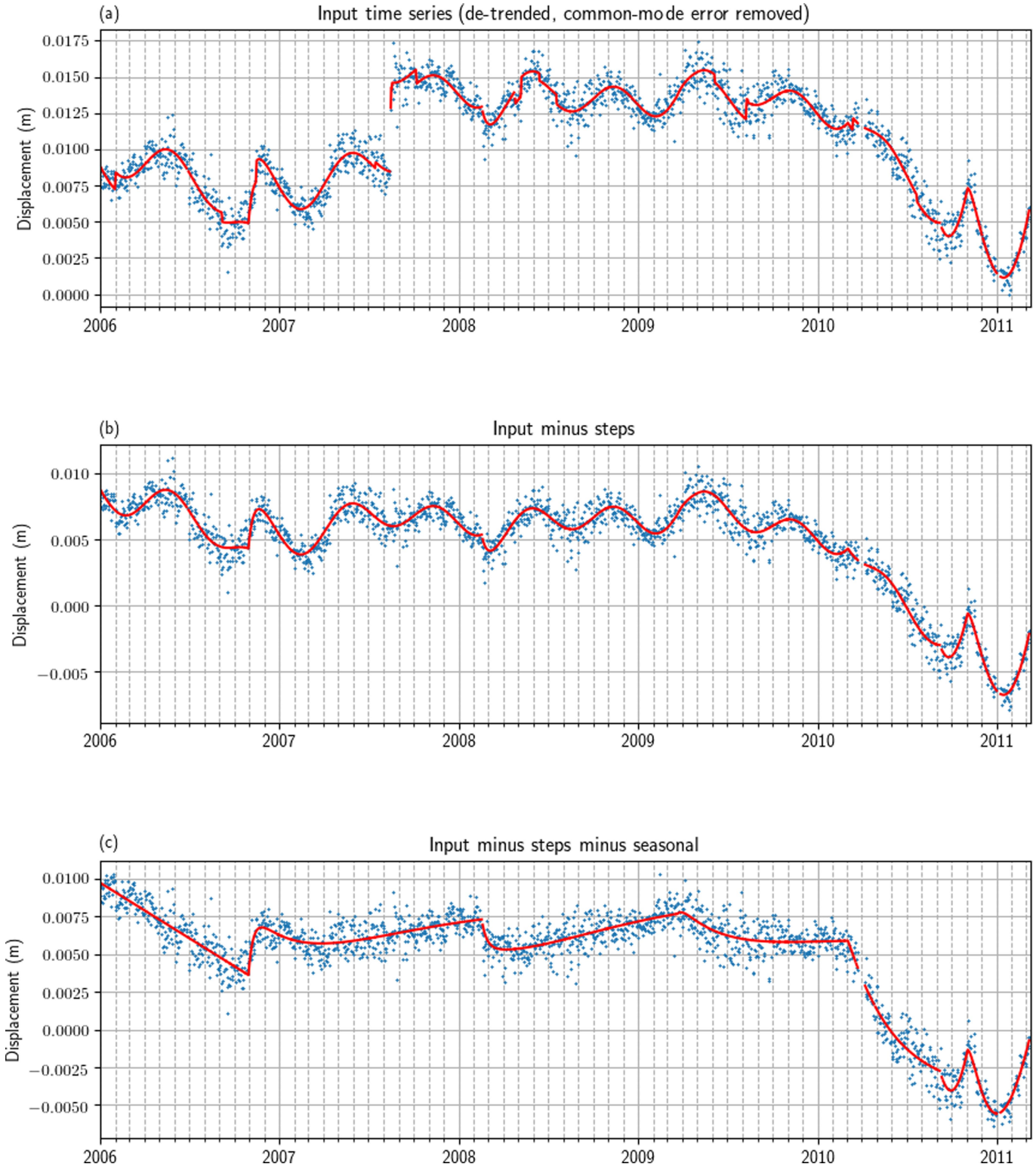

Extended Data Fig. 5 | The corrections to the time series made possible after application of the regression model solved by GrAtSiD. a, The example time series is for the East component of station Ooamishirasato in Japan. Blue dots show the time series input into the GrAtSiD routine. This time series has been corrected for the common-mode error. The red line shows the complete fit of the regression model solved by GrAtSiD. This includes steps, oscillation terms, the first-order polynomial and the multi-transients. The time series has been optimally tilted (detrended) for clarity of presentation. **b**, The time series (blue dots) and trajectory model (red line) after removal of the modelled step offsets. **c**, The time series and the regression model following the removal of the modelled seasonal and step terms. The remaining terms in the model are the first-order polynomial and multi-transients. It is these detrended modelled trajectories following seasonal and step removal (shown in panel **c** in red) that are represented in Supplementary Videos 3–8 and Figs. 3 and 4 and Extended Data Fig. 4.

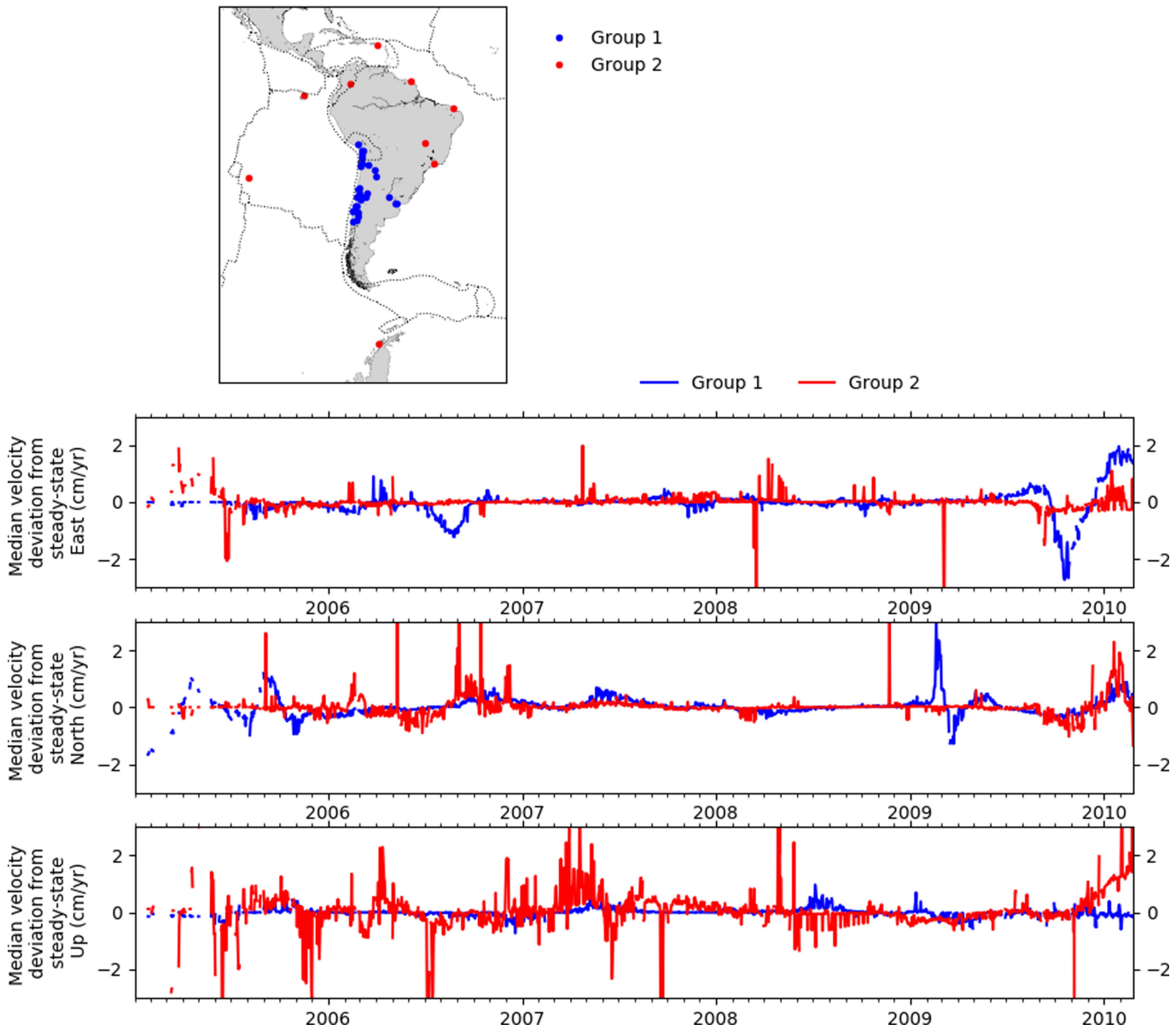

Extended Data Fig. 6 | Investigating spatial extents of the pre-Maule-earthquake wobbling in the network solutions. The map shows the locations of two groups of stations used in the investigation into spatial extent of the unstable period observed before the Maule earthquake. The time series show the average (median) deviation from median velocity at each station of the two groups in the above map for each directional component, where the median velocity of each station is determined between 1 January 2005 and 25 February 2010.

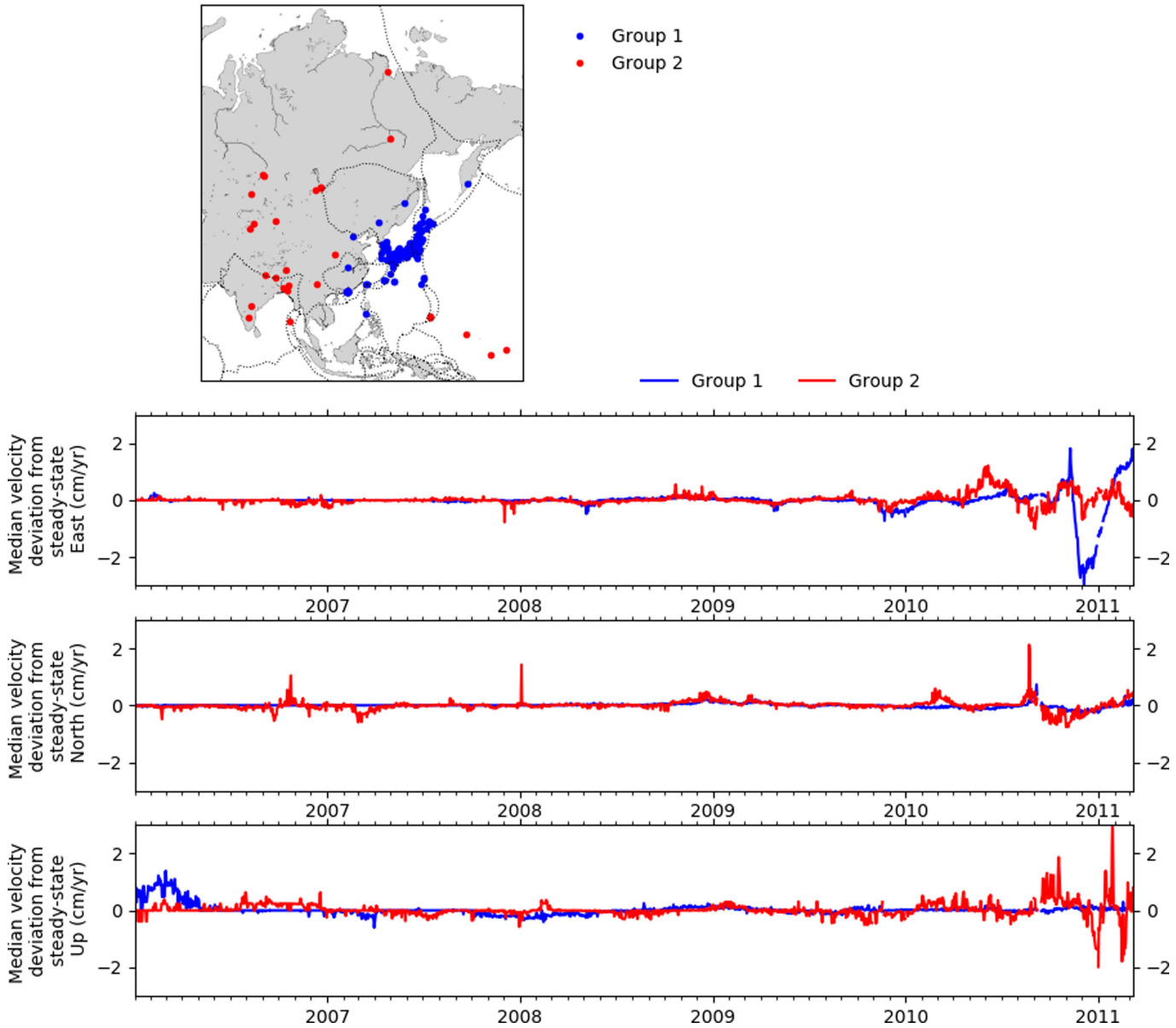

Extended Data Fig. 7 | Investigating spatial extents of the pre-Tohoku-oki-earthquake wobbling using the Nevada Geodetic Laboratory's IGS08 PPP solutions. The map shows the locations of two groups of stations used in the investigation into spatial extent of the unstable period observed before the Tohoku-oki earthquake. The time series show the average (median) deviation from median velocity at each station of the two groups in the above map for each directional component, where the median velocity of each station is determined between 1 January 2006 and 8 March 2011.

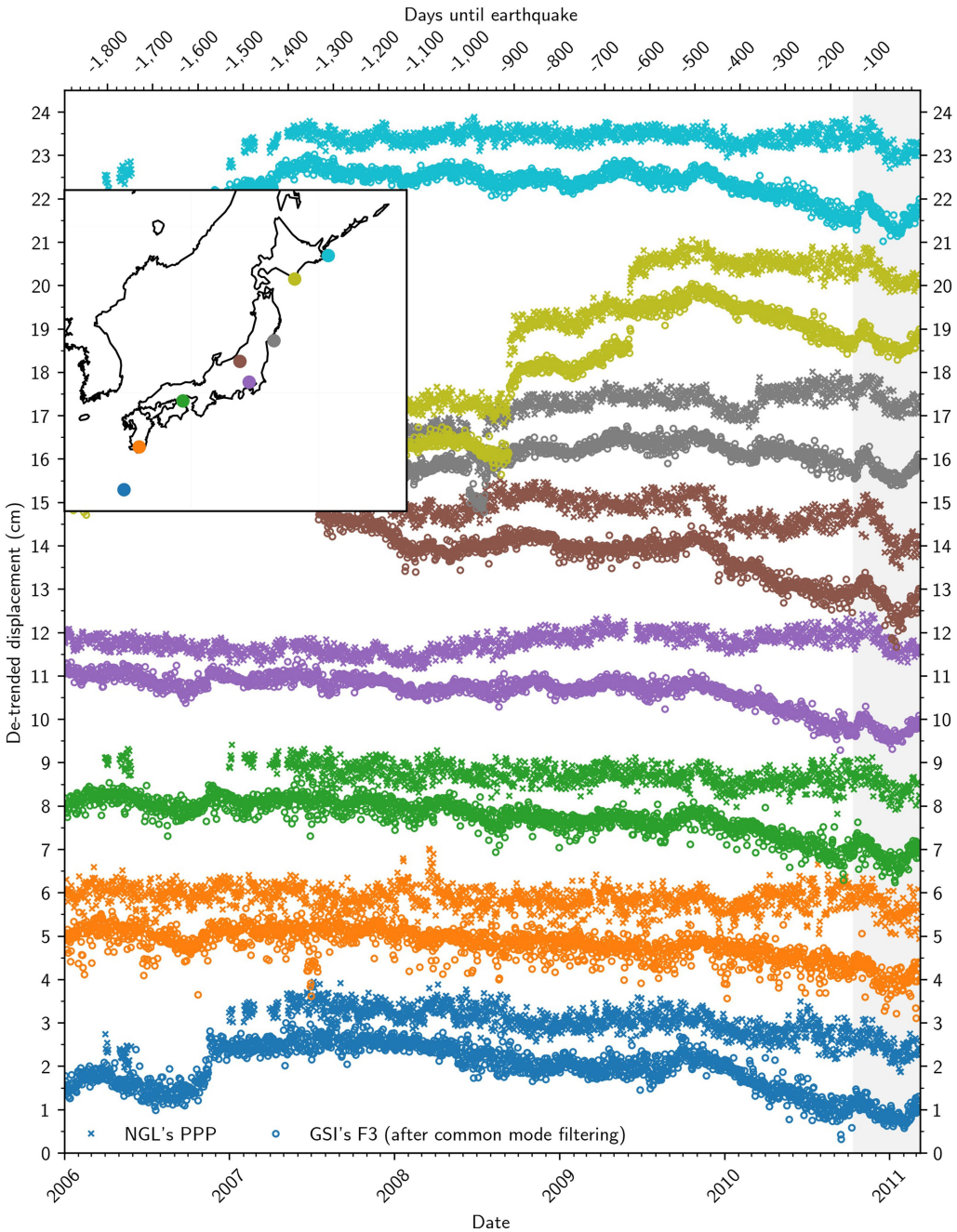

Extended Data Fig. 8 | Comparison of GSI's F3 solutions with NGL's IGS08 PPP solutions for selected stations across Japan before the Tohoku-oki earthquake. All time series shown are in the East component. Circles show the F3 and crosses show the PPP solutions. Colours correspond to the stations located on the inset map.

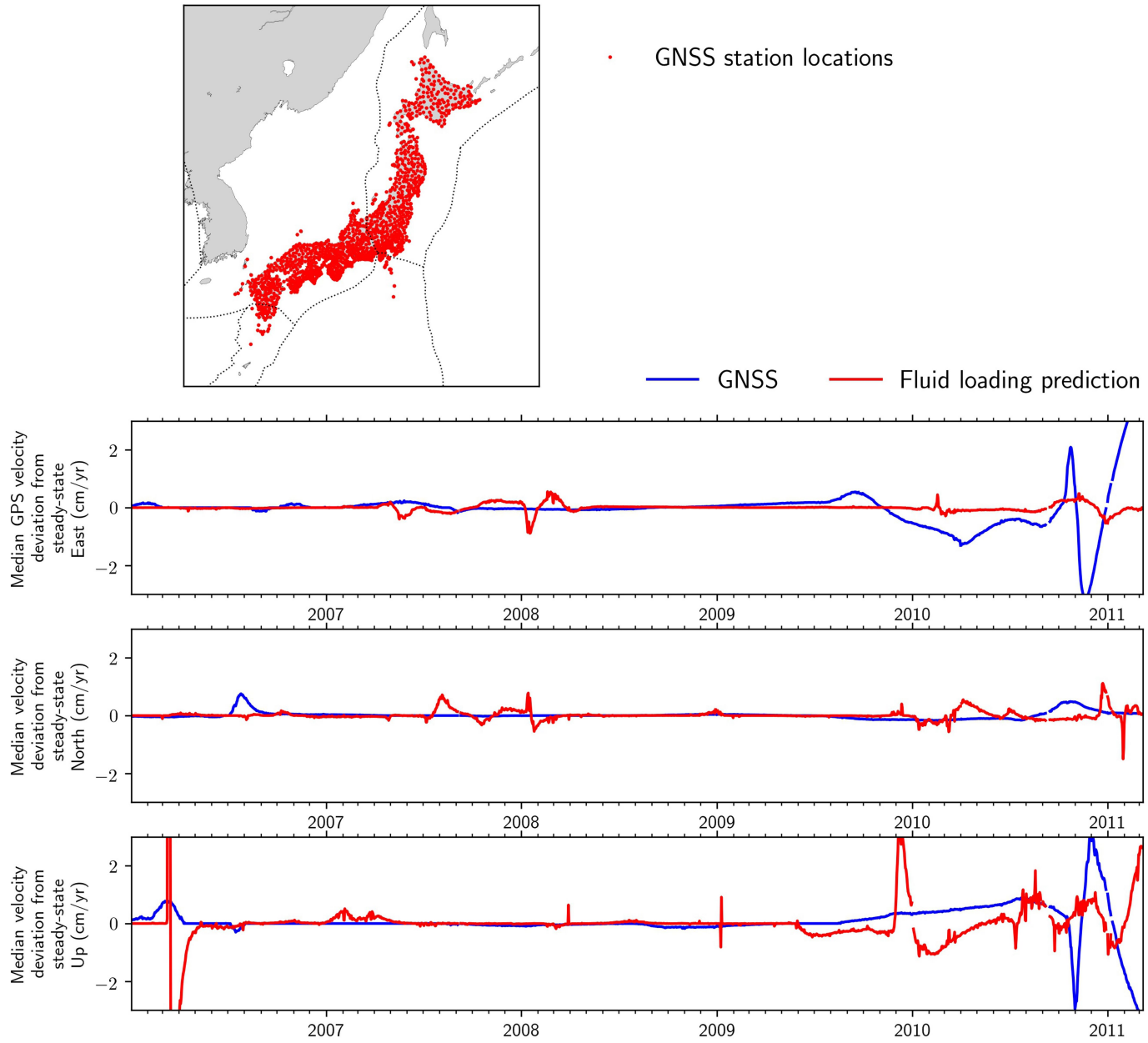

Extended Data Fig. 9 | Comparing the transient surface motions recorded by GNSS and predicted by fluid-loading models before the Tohoku-oki earthquake. The map shows the GNSS station locations used in the analysis comparing fluid-loading displacement predictions to GNSS displacement measurements for the pre-Tohoku-oki case. The time series show a comparison of the median velocity variations for GNSS-measured (GSI's F3 solutions) and fluid-loading-predicted displacements at the locations in the map. Velocities are taken from the trends estimated by GrAtSiD. In the horizontal components, the prediction from fluid loading produces much lower velocities than those observed. In the vertical component, there is considerable deviation from steady-state velocity in both the GNSS observation and fluid-loading prediction but with visibly low agreement in sense of motion.

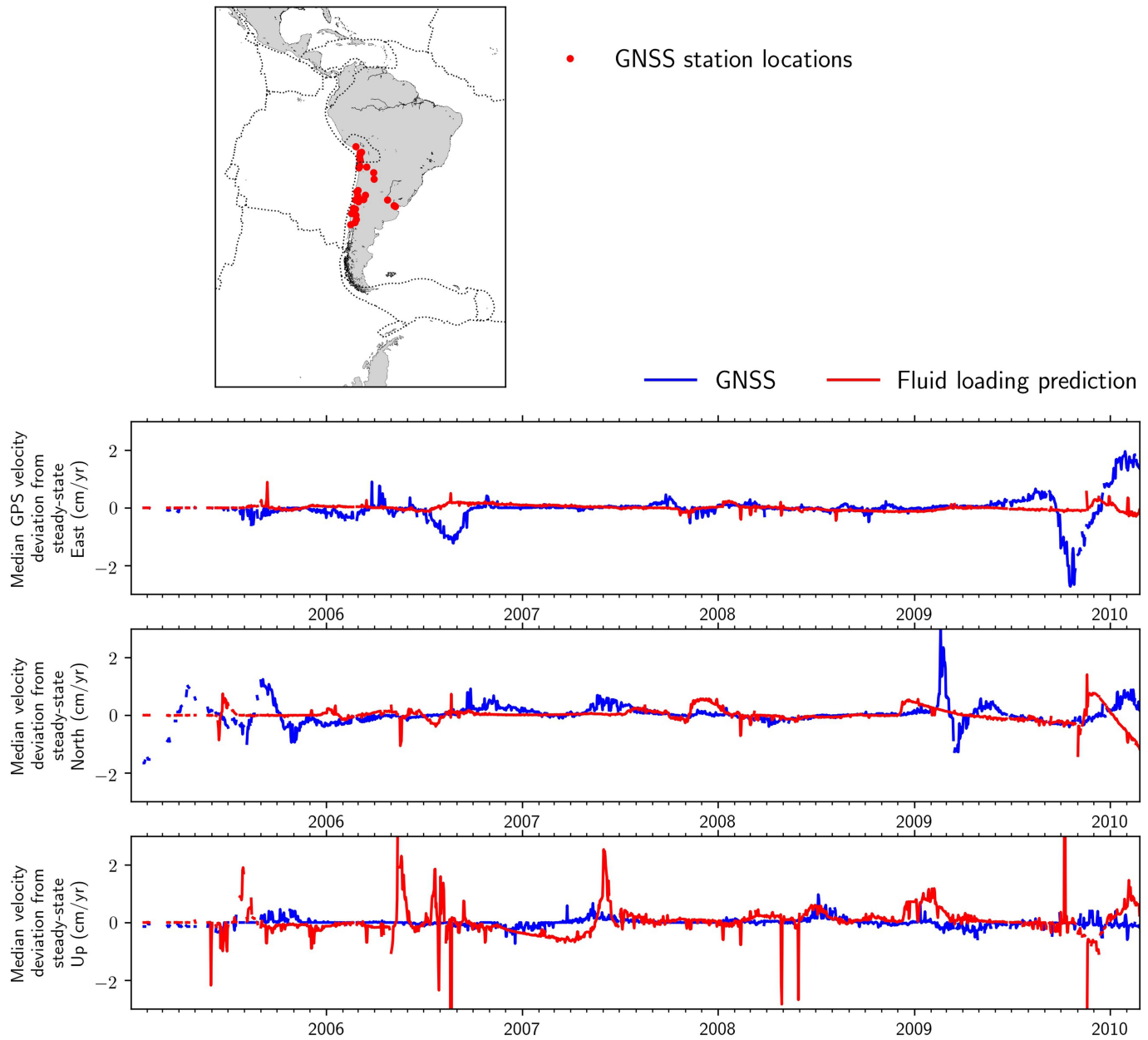

Extended Data Fig. 10 | Comparing the transient surface motions recorded by GNSS and predicted by fluid-loading models before the Maule earthquake. The map shows the GNSS station locations used in the analysis comparing fluid-loading displacement predictions to GNSS displacement measurements for the pre-Maule case. The time series show a comparison of the median velocity variations for GNSS-measured and fluid-loading-predicted displacements at the locations in the map. Velocities are taken from the trends estimated by GrAtSiD. In the East component (in which the pre-Maule unstable motion is most pronounced) the prediction from fluid loading produces much lower deviation from steady-state velocities than those observed by GNSS.